FOI-R--0177--SE
September 2001
ISSN 1650-1942
Technical report

Lars M.H. Ulander, Björn Larsson, Anders Gustavsson,
Per-Olov Frölind, Tommy Jonsson, Gunnar Stenström

RAMCAR-98

CARABAS VHF-band SAR

Final report

Sensor Technology
SE-581 11 Linköping

SWEDISH DEFENCE RESEARCH AGENCY

Sensor Technology
P.O. Box 1165
SE-581 11 Linköping

FOI-R--0177--SE

September 2001

ISSN 1650-1942

Technical report

Lars M.H. Ulander, Björn Larsson, Anders Gustavsson,
Per-Olov Frölind, Tommy Jonsson, Gunnar Stenström

RAMCAR-98

CARABAS VHF-band SAR

Final report

Issuing organization	Report number, ISRN	Report type
FOI – Swedish Defence Research Agency Sensor Technology P.O. Box 1165 SE-581 11 Linköping	FOI-R--0177--SE	Technical report
	Research area code 4. C4ISR	
	Month year September 2001	**Project no.** E3029
	Customers code 5. Contracted Research	
	Sub area code 42 Surveillance Sensors	

Author/s (editor/s)	Project manager
Lars M.H. Ulander Björn Larsson Anders Gustavsson Per-Olov Frölind Tommy Jonsson Gunnar Stenström	Lars M.H. Ulander **Approved by** **Scientifically and technically responsible** Lars M.H. Ulander

Report title

RAMCAR-98. CARABAS VHF-band SAR. Final report.

Abstract (not more than 200 words)

The French-Swedish RAMCAR-98 experiment was conducted in May 1998 at two test sites in southern France. The Swedish CARABAS-II VHF-band SAR participated together with the French RAMSES multi-frequency SAR. This report summarises the data collection as well as processing and analysis of the CARABAS images.

Data from all flight tracks have been successfully processed and the radiometric calibration is based on in-scene reference trihedrals. Image quality varies slightly from image to image. The main problems encountered are due to antenna back-lobe leakage but the quality also depends on the success of filtering the radio-frequency interference.

The radar-cross section of deployed vehicle targets, located both in the open and under foliage, was measured for different aspect and incidence angles. All measurements varied in the range 1-20 dBm^2, with the smallest values observed for vehicles in forest concealment and for the largest incidence angle. Trihedrals deployed inside different forest stands enabled the two-way attenuation to be measured, giving a maximum value of 2.9 dB.

Change detection was found to be a robust method for concealed target detection in CARABAS images since the radar backscattering from trees and other natural objects is relatively low and has a high spatial and temporal correlation.

Keywords

CARABAS, SAR, VHF, foliage penetration, ground surveillance, radar cross section, change detection

Further bibliographic information	Language English
ISSN 1650-1942	**Pages** 67 p.
	Price acc. to pricelist **Security classification**

Utgivare Totalförsvarets Forskningsinstitut - FOI Sensorteknik Box 1165 581 11 Linköping	**Rapportnummer, ISRN** FOI-R--0177--SE	**Klassificering** Teknisk rapport
	Forskningsområde 4. Spaning och ledning	
	Månad, år September 2001	**Projektnummer** E3029
	Verksamhetsgren 5. Uppdragsfinansierad verksamhet	
	Delområde 42 Spaningssensorer	
Författare/redaktör Lars M.H. Ulander Björn Larsson Anders Gustavsson Per-Olov Frölind Tommy Jonsson Gunnar Stenström	**Projektledare** Lars M.H. Ulander	
	Godkänd av	
	Tekniskt och/eller vetenskapligt ansvarig Lars M.H. Ulander	

Rapportens titel (i översättning)

RAMCAR-98. CARABAS VHF-band SAR. Slutrapport.

Sammanfattning (högst 200 ord)

En fransk-svensk mätkampanj, RAMCAR-98, genomfördes vid två olika testområden i södra Frankrike under maj månad 1998. Den svenska flygburna SAR sensorn CARABAS-II, opererande på VHF-bandet, deltog tillsammans med det franska flerfrekvenssystemet RAMSES. Föreliggande rapport sammanfattar insamlingen och analysen av radardata registrerade med CARABAS-II.

SAR-bilder från CARABAS-II har kunnat genereras från samtliga mätlöpor och vid den radiometriska kalibreringen utnyttjas utplacerade hörnreflektorer inom det avbildade området. Bildkvalitén varierar något från bild till bild. Den främsta orsaken är otillräcklig undertryckning av radarsignaler från antennens backlob men även förmågan att identifiera och eliminera externa radiosignaler påverkar kvalitén.

Radarmålarean för utplacerade fordon i såväl öppen terräng som dolda under en vegetationsmask har räknats fram ur SAR-bilderna för olika aspekt- och infallsvinklar. Mätvärdena varierar mellan 1-20 dBm^2, med de lägsta målareorna uppmätta för fordon i skog på störst infallsvinkel. Från trihedraler utplacerade i olika skogsbestånd har tvåvägsdämpningen genom vegetationen kunnat uppskattas och den högsta siffran som erhållits är 2.9 dB. Förändringsdetektion har visat sig vara en robust metod att med CARABAS-sensorn upptäcka mål som gömts undan i skydd av vegetation. Det huvudsakliga skälet till detta är att returspridningen från träd och andra naturliga objekt är relativt låg och uppvisar en hög rumslig och temporal korrelation.

Nyckelord

CARABAS, SAR, VHF, vegetationsgenomlysning, markmålsspaning, radarmålarea, förändringsanalys

Övriga bibliografiska uppgifter	**Språk** Engelska
ISSN 1650-1942	**Antal sidor:** 67 s.
Distribution enligt missiv	**Pris: Enligt prislista** **Sekretess**

TABLE OF CONTENTS

1. Introduction

There is a high military interest of detecting man-made targets concealed under foliage or camouflage. Recent conflicts, e.g. the Kosovo crisis in 1999, have shown the importance of developing new operational sensors with such capability. Presently, the most promising airborne sensor for this application is low-frequency (< 1 GHz) synthetic-aperture radar (SAR). By using low radar frequencies it is possible to reduce the backscattering and attenuation due to vegetation and thereby enable detection of concealed man-made objects. The low frequencies also make radar camouflage techniques, e.g. radar nets and stealth design, less useful. Past experience, however, has shown that these systems require the finest possible resolution, which calls for ultra-wideband (UWB) SAR, i.e. the fractional bandwidth is close to unity. This means that the resolution is finer than the centre wavelength used.

The amount of experimental data to assess the performance of low-frequency SAR in different conditions is rather limited. A joint Swedish-French experiment was therefore conducted in May 1998 with the objective of evaluating different frequency bands for concealed target detection. From France, ONERA participated with the RAMSES airborne SAR operating at L- and X-band. From Sweden, FOA participated with the CARABAS-II airborne SAR operating in the low VHF region (20-90 MHz). Both SAR systems collected data over two test sites (Les Landes and Lozère) located in southern France during a two week period in May 1998. SAR data have later been analysed and the present report describes the work performed by FOA within the collaborative effort.

Besides the military application there is also a high interest of using low-frequency SAR for forest mapping, in particular for biomass and stand volume retrieval. The two test sites provided an excellent opportunity to collect data over different forests and to investigate the forest mapping capability. Collection of *in situ* data of the forest and ground conditions was performed by French scientists from LCT in Montpellier and CESBIO in Toulouse.

On 1 January 2001 there was a merger between the Aeronautical Research Institute (FFA) and the Defence Research Establishment (FOA). The new organisation is the Swedish Defence Research Agency, FOI. The former name FOA will, however, be used in this report.

2. CARABAS VHF-band SAR

CARABAS-II is an airborne UWB and wide-beam SAR operating in the VHF-band between 20 and 90 MHz. The polarisation is mainly horizontal on both transmit and receive, and the spatial resolution of the images is about 2.5 m x 2.5 m. The system implementation is based on the experiences gained using the predecessor CARABAS-I and includes a number of major changes to improve system performance. The first test flights were made in October 1996, and the development has been a joint effort together with Ericsson Microwave Systems AB. The design of an UWB SAR system operating in this frequency interval is a challenging task in many respects. Several special considerations have influenced the design such as the imaging geometry for a wide-beam SAR instrument, the electromagnetic coupling of the antenna with the airframe, and the presence of strong radio-frequency interference (RFI) [1-4]. Conventional principles for radar system analysis have been revisited and adapted to the characteristics of an UWB and wide-beam low frequency SAR.

The most striking part of the realization is the antenna arrangement. In order to retain low ohmic losses, the length of the antenna needs to be close to half the wavelength and this has been accomplished with two rigid Kevlar push booms mounted in front of the nose of the Sabreliner aircraft as shown in Figure 1.

Figure 1. The Sabreliner aircraft, owned and operated by FMV:Prov, with the antenna system for CARABAS-II installed. (Courtesy: FMV:Prov).

The antennas are designed to provide essentially horizontal polarization and omni-directional illumination across the 20-90 MHz band. Each boom is 8 m long in total, with the 5 m long active part extending in front of the aircraft nose, and the boom separation is 1.85 m. Both antennas are fed during transmission and a delay line is used to tilt the antenna beam to the left- or right-hand side of the flight track. On receive, the signals from each antenna are simultaneously recorded in two parallel receiver channels. The poor directivity of the antenna system, i.e. the wide-beam characteristics, means that objects on the ground will be illuminated over a very wide aspect angle, typically 90 degrees or more. Ideally, an illumination width of 180° is present and a circular average over a semicircle segment represents each raw data sample acquired along the flight path, as is illustrated in Figure 2. In reality the sensitivity of the antenna pattern will fluctuate with respect to frequency, incidence

angle and aspect angle. The suppression between the left- and right-hand side is also limited and will cause ambiguities. These will appear as artifacts in the processed image of the illuminated scene and are caused by strong scatterers from the opposite side which are folded into the image and positioned at the corresponding distance. They are, however, not as well focused due to the mismatch in the motion compensation, which adjusts data with respect to the true side and this makes it possible to identify them rather easily.

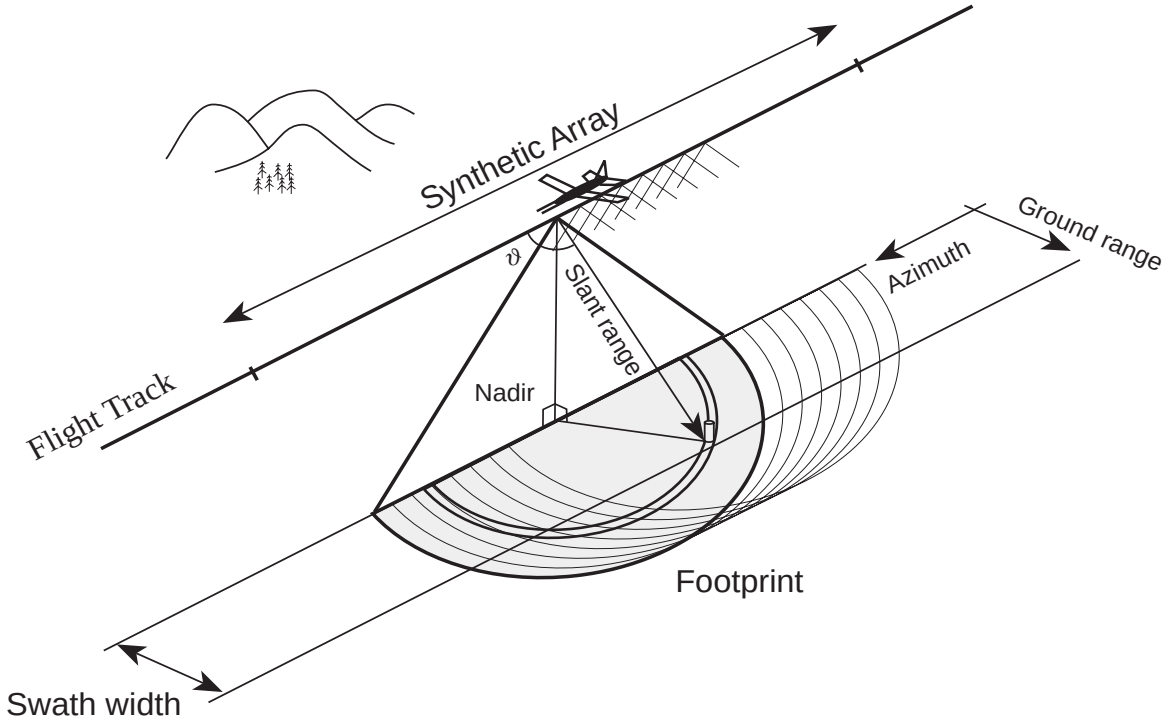

Figure 2. The basic imaging geometry for CARABAS-II. To obtain a sufficient resolution in azimuth the signal must be integrated over a large aspect angle. The effective swath in the final image is thus reduced compared to the raw data coverage required to carry out the corresponding inverse processing.

Operating a wide-beam SAR system at high altitudes will thus give a synthetic aperture length of tenths of kilometers. The signal processing algorithms must therefore handle long data segments in azimuth to utilize the Doppler information fully, and this puts requirements on the accuracy and temporal drift of the navigation system to carry out the motion compensation properly. The platform fluctuations in CARABAS-II are monitored with a carrier-phase differential GPS (CDGPS) device. The ground based CDGPS receiver is deployed within or in the vicinity of each test site.

The weak radar returns collected along the synthetic aperture are competing with many strong interference signals found within the total radar band 20-90 MHz, and will require a receiving chain which combines a high sensitivity with a very large dynamic range to avoid saturation effects. A dynamic range in the order of 80-90 dB is typically needed. The difficult RFI environment will be further manifested when operating the system from high altitudes where an increasing number of sources will appear within line-of-sight. A favourable way of improving the dynamic range of a system is to use an instantaneous narrow bandwidth. In this

way, sharp filters can be used in the IF section of the receiver and the demand for high speed sampling is limited. The full bandwidth is generated by a stepped-frequency scheme in combination with linear FM pulses (chirps). This technique also allows for transmitting the higher frequencies more often than the lower ones along the flight path. In this way the Nyquist along-track sampling requirement is fulfilled at each frequency instead of being imposed by the maximum transmitted frequency only [1, 3].

The receiver in CARABAS-II has a spurious-free dynamic range of 88 dB. The frequency stepping scheme is fully programmable and one can also define a listening mode, with the radar transmission inhibited, and thus only register the competing RFI contributions within each frequency sub-band. By repeating this sniffing procedure periodically for all sub-bands along the synthetic aperture the temporal fluctuations of the interfering signals will be recorded and can be used as estimates in the RFI suppression of the radar raw data [5-6]. Figure 3 gives an example of the synthesised wideband spectrum received far out in range, i.e. at a fairly shallow incidence angle, where the radar return is rather weak compared to the RFI signals. The registration was made during the EUFORA field campaign in Finland, September 1997. In this experiment the radar transmission was only approved within the interval 25-88 MHz. In addition to the interference signals the nadir return at VHF-band is in general very strong since most ground surfaces give a mirror-like echo. This part of the illuminated scene is typically 50-70 dB stronger than the rest of the image.

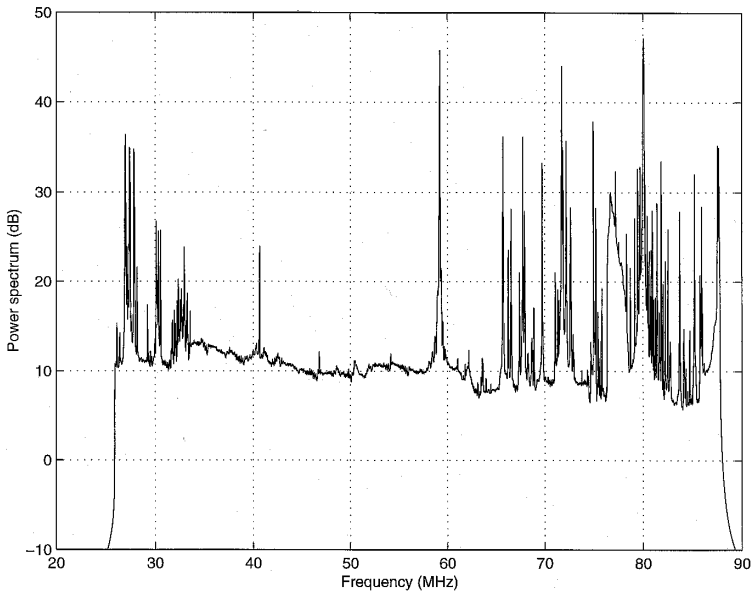

Figure 3. A typical power spectrum acquired with CARABAS-II and sampled far out in range compared to nadir. In this region the radar return is weak and the RFI signals dominate.

The main disadvantage of using the stepped-frequency technique is the problem of controlling paired-echo sidelobes, which may give a considerable degradation of the image quality. They are caused by the pulse compression algorithm if any significant periodic amplitude or phase ripple remain in the reconstructed wideband spectrum. The effect generates false bright spots in range centred around the true response of a major scatterer. A stable system and careful calibration is required in order to reduce the effect to a satisfactory level. A calibration methodology with the purpose of reducing this effect during processing has been derived. It is based on an optimal linear filter, which maximizes signal-to-noise ratio under the constraint

of a flat output energy spectrum [7]. The impact on the peak-sidelobe-ratio from a small sinusoidal amplitude or phase error can be quantified to less than 0.5 dB or 4 degrees peak-to-peak, respectively, to keep the ratio below -30 dB. This places a stringent requirement on system stability and calibration.

An increase of the transmitted power is one obvious way to change and improve the overall system performance. To avoid an interference conflict in that case it is important, however, that the system can adapt to the present signal environment and generate an instantaneous total radar spectrum with sharp, narrow band and deep notches at channels occupied by vital services, e.g. air traffic control or telemetry. A programmable and flexible waveform generator, which can shape the spectrum arbitrarily, is thus a key component. Figure 4 gives an example of the synthesised wideband power spectrum received from nadir in range and with a deep notch in the radar transmitted signal at 75 MHz, a frequency allocated by an ILS beacon for air traffic control. The registration was made at the calibration test site Visingsö in Sweden with a fresh water lake surface illuminated at nadir. The same restrictions of the radar transmission were applied as in Figure 3. The overall shape for the envelope of the power spectrum in Figure 4 with a decreasing value for higher frequencies, can be explained from the two identical signals transmitted by the two geometrically separated antennas, but with a fix time delay in between, and in this case interfering along the nadir direction. The spiky pattern is the received and superimposed RFI signals, which is clearly seen in the upper end where the FM radio band begins. The reason of the relatively slow and small remaining modulations is caused by the antenna characteristics. At both test sites during the RAMCAR-98 experiment the notch at 75 MHz was the only one applied.

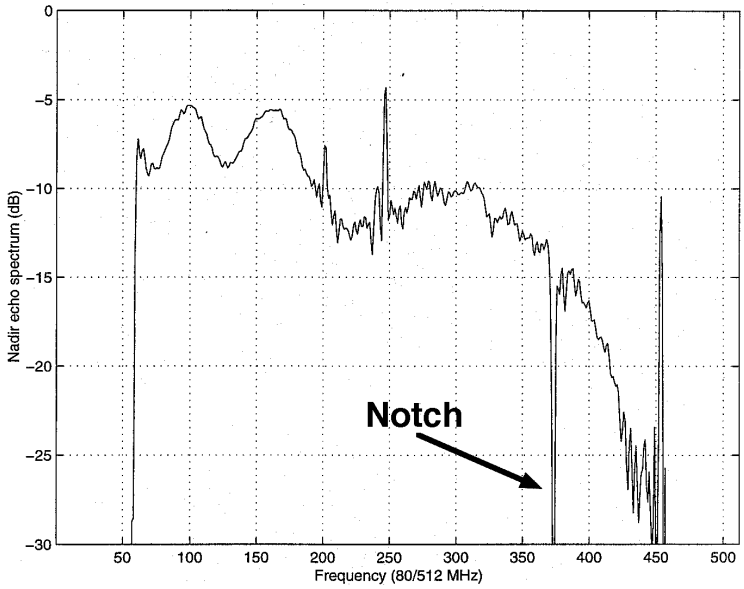

Figure 4. The synthesised wideband strong nadir echo spectrum, in this case limited to 25-88 MHz. A deep notch has been programmed in the waveform generator at the frequency 75 MHz and is clearly visible in the received spectrum.

The flow of digital samples from the two receiver units gives a maximum sustained data rate of 160 Mbit/s and is recorded on high density digital tape (HDDT) cartridges. Data are taken as 14 bit samples at a sampling rate of 5 MSample/s in each receiver channel. The data are formatted, tagged with system information and fed to the tape recorder in 8 bit format. There

is no real-time processing on board. On ground all recorded data are transcribed to a tape medium more convenient to handle, i.e. digital linear tape (DLT) cartridges. The main part of the processing software is implemented in C-code and runs on powerful UNIX workstations.

An overall system block diagram of the radar hardware is given in Figure 5. To obtain a fully coherent CARABAS-II system the direct digital synthesiser (DDS) is used to generate the local oscillator signal for both the transmitter and the two receivers. In the transmit chain the local oscillator is used in the final mixing stage so that the arbitrary waveform generator signal is allocated to the selected carrier frequency. The FM chirp pulse is amplified by the power amplifier to approximately 500 W. By the antenna selection network the signal is then fed to both the left- and right-hand side antenna. In one of the feeders a delay line is inserted to give the phase shift needed to steer the beam to the selected side. Simultaneously, a -50 dB signal sample is taken from the power amplifier to be used as a calibration signal. The receivers are trailing the transmitter while stepping across the band. The effective PRF is about 200 Hz when covering the full bandwidth.

The system main parameters used to configure the CARABAS-II radar operation during RAMCAR-98 can be found in chapter 3, i.e. Tables 1 and 4.

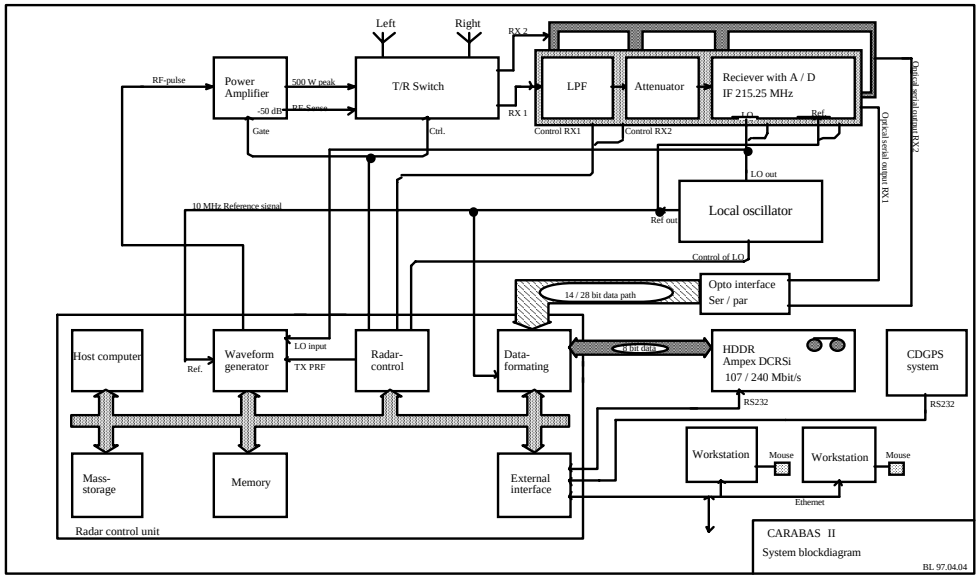

Figure 5. System block diagram of CARABAS-II.

3. Flight program

The CARABAS aircraft left Sweden in the morning May 11 and landed at the Cazaux air base about noon the same day and a flight crew briefing was held in the afternoon. Two test areas had been selected earlier as shown in Figure 6:

- Les Landes: Nezer forest (Maritime pine) close to the air base of Cazaux.
- Lozère: Causse Mende forest (mixture, but predominantly Austrian pine) located in the ”Massif Central” near the town Mende.

Figure 6. Map over France giving the locations of the two target areas.

Four flight days were planned for CARABAS. Two days over the Les Landes forest, i.e. May 12 and May 14, and two days over the selected target area in Lozère, i.e. May 18 and 19. All flights were carried out according to plan. Figures 7-10 show the different areas of interest.

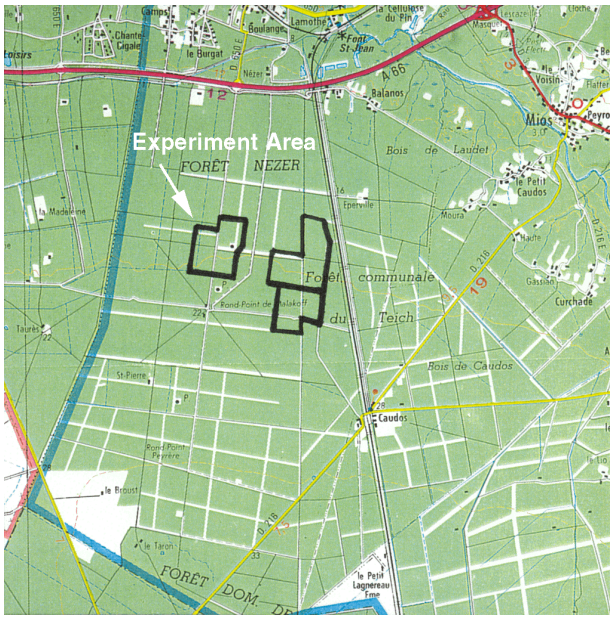

Figure 7. Nezer forest in Les Landes with three possible test areas delineated in black. The upper-left area (size about 1 km^2) was selected for the RAMCAR-98 experiment.

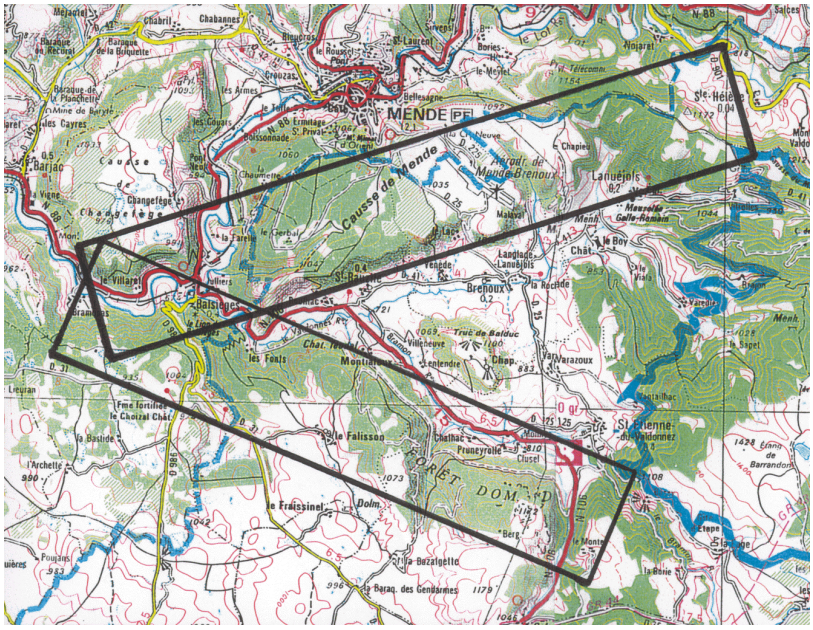

Figure 8. Planned flight coverage in the Causse Mende and Causse Sauveterre area in Lozère. The city of Mende is located just north of Causse Mende. The delineated swaths are about 2 km wide.

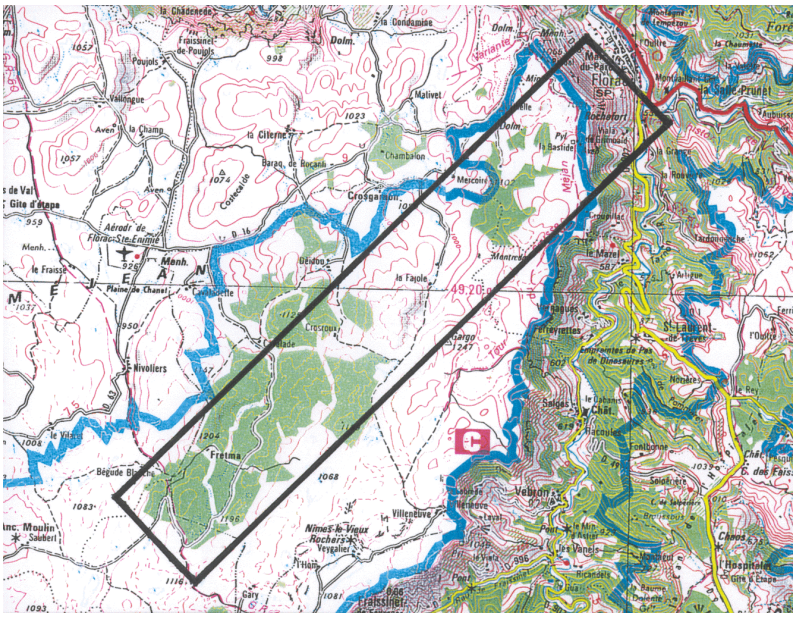

Figure 9. Planned flight coverage in the Causse Mejean area in Lozère. The city of Florac is located north-east of Causse Mejean. This area is located about 20 km south of the city of Mende. The delineated swath is about 2 km wide.

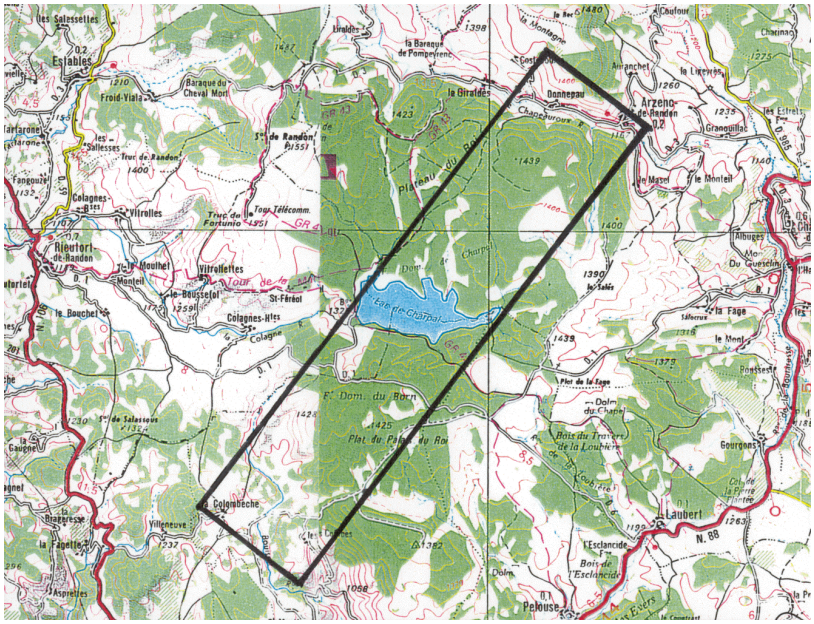

Figure 10. Planned flight coverage in the Lac de Charpal area in Lozère. This area is located about 10 km north of the city of Mende. The delineated swath is about 2 km wide.

3.1 Les Landes missions

The CARABAS system parameters for the Les Landes missions are summarised in Table 1. In practise, the waveform used for mission 1 was slightly different due to an error when creating the radar control micro-code. Re-calibration of the radar system was therefore required before good SAR images could be generated.

Table 1. CARABAS system parameters: Mission fr98_1 & fr98_2 - All passes.

Number of frequency steps	37
Frequency step size	1.875 MHz
First centre frequency	21.25 MHz
Last centre frequency	88.75 MHz
RFI sniff	Yes, every 37th transmit pulse
Pulse type	Chirp
Pulse length	5 μs
Frequency notch	74.8 – 75.3 MHz
Number of receiver channels	2
ADC sampling rate	5 MHz
Range samples	720
PRF	5952 Hz
Radar acquisition time	178 s

The basic flight pattern included eight flight tracks with the same nominal incidence angle but with varying track directions. The flight altitude was always FL 100, i.e. about 3000 m. On the first day, two extra tracks over the Nezer forest were included with a different incidence angle, i.e. the parallel but offset tracks 9 and 10 in Figure 11. The main flight parameters derived from the mission planning software are summarised in Table 2. On the second day, two extra tracks collected data over Dune de Pyla which is located on the Atlantic shoreline west of the Nezer forest. They are identified as tracks 9 and 10 in Figure 12 and also differ with respect to the incidence angle. The full flight program for mission 2 is given in Table 3.

Table 2. Flight plan May 12.

Pass	Begin	End	Heading	Alt	Lenght
1	N44°37'38" W1°11'20"	N44°35'55" W0°51'50"	097°	FL100	14 nmi
2	N44°32'06" W0°52'30"	N44°33'48" W1°11'59"	277°	FL100	14 nmi
3	N44°40'38" W1°08'08"	N44°32'11" W0°52'27"	127°	FL100	14 nmi
4	N44°29'06" W0°55'42"	N44°37'33" W1°11'23"	307°	FL100	14 nmi
5	N44°42'05" W1°03'16"	N44°29'10" W0°55'36"	157°	FL100	14 nmi
6	N44°27'39" W1°00'34"	N44°40'34" W1°08'14"	337°	FL100	14 nmi
7	N44°41'36" W0°58'02"	N44°27'40" W1°00'26"	187°	FL100	14 nmi
8	N44°28'08" W1°05'47"	N44°42'04" W1°03'24"	007°	FL100	14 nmi
9	N44°30'13" W0°52'50"	N44°31'56" W1°12'18"	277°	FL100	14 nmi
10	N44°28'22" W1°08'23"	N44°42'18" W1°06'01"	007°	FL100	14 nmi

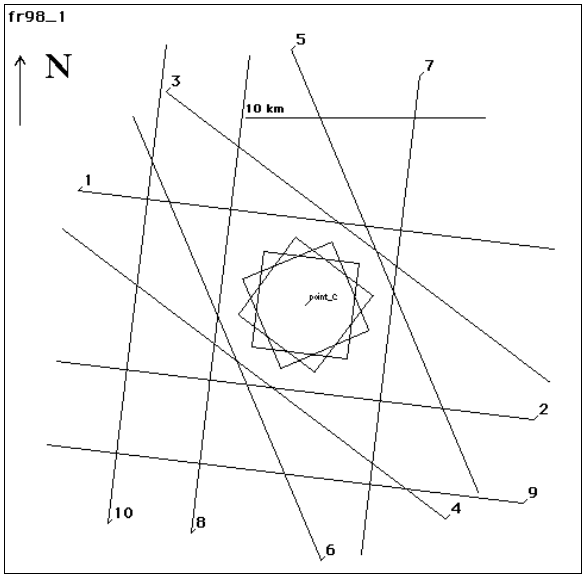

Figure 11. Flight plan for mission 1 on 12 May 1998.

Table 3. Flight plan May 14.

Pass	Begin	End	Heading	Alt	Lenght
1	N44°37'38" W1°11'20"	N44°35'55" W0°51'50"	097°	FL100	14 nmi
2	N44°32'06" W0°52'30"	N44°33'48" W1°11'59"	277°	FL100	14 nmi
3	N44°40'38" W1°08'08"	N44°32'11" W0°52'27"	127°	FL100	14 nmi
4	N44°29'06" W0°55'42"	N44°37'33" W1°11'23"	307°	FL100	14 nmi
5	N44°42'05" W1°03'16"	N44°29'10" W0°55'36"	157°	FL100	14 nmi
6	N44°27'39" W1°00'34"	N44°40'34" W1°08'14"	337°	FL100	14 nmi
7	N44°41'36" W0°58'02"	N44°27'40" W1°00'26"	187°	FL100	14 nmi
8	N44°28'08" W1°05'47"	N44°42'04" W1°03'24"	007°	FL100	14 nmi
9	N44°29'55" W1°19'49"	N44°42'19" W1°10'39"	028°	FL100	14 nmi
10	N44°30'48" W1°22'09"	N44°43'12" W1°12'59"	028°	FL100	14 nmi

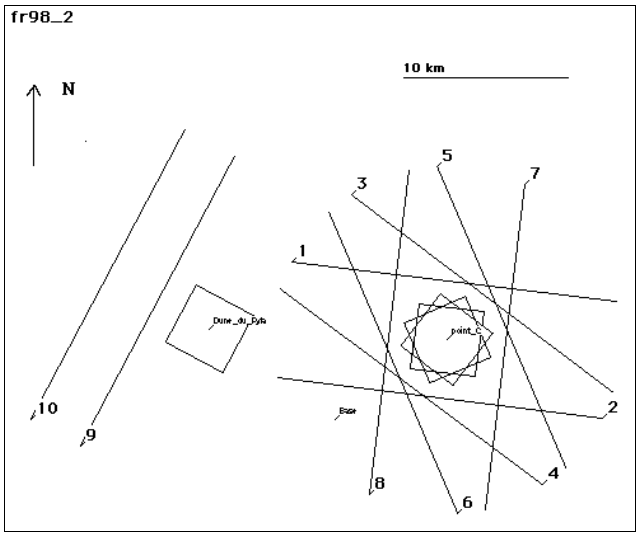

Figure 12. Flight plan for mission 2 on 14 May 1998.

3.2 Lozère missions

The CARABAS system parameters for the Lozère missions are summarised in Table 4.

Table 4. CARABAS system parameters: Mission fr98_3 & fr98_4 - All passes.

Number of frequency steps	37
Frequency step size	1.875 MHz
First centre frequency	21.25 MHz
Last centre frequency	88.75 MHz
RFI sniff	Yes, every 37th transmit pulse
Pulse type	Chirp
Pulse length	5 μs
Frequency notch	74.8 – 75.3 MHz
Number of receiver channels	2
ADC sampling rate	5 MHz
Range samples	720
PRF	5952 Hz
Radar acquisition time	236 s

The flight pattern included nine flight tracks with varying incidence angle and track direction over three different areas: Causse Mende (and Sauveterre), Causse Mejean (Florac), and Lac de Charpal. The flight altitude was FL 150, i.e. about 4500 m, which resulted in a height above the aim point of about 3500 m. On the first day, five tracks were flown over the Causse Mende area and four tracks over the Causse Mejean area as shown in Figure 13. On the second day, eight tracks were flown over the Causse Mende area and one track over Lac de Charpal area as shown in Figure 14.

Pass number 10 on May 19 was not flown due to aircraft endurance limitations. All other passes were flown and data were successfully collected. The main flight parameters are found in Tables 5 and 6.

Table 5. Flight plan May 18.

Pass	Begin	End	Heading	Alt	L
1	N44°34'39" E3°40'41"	N44°28'39" E3°14'51"	252°	FL151	19 nmi
2	N44°24'22" E3°16'49"	N44°30'22" E3°42'37"	072°	FL151	19 nmi
3	N44°20'59" E3°35'54"	N44°39'27" E3°27'32"	342°	FL151	19 nmi
4	N44°38'03" E3°21'32"	N44°19'35" E3°29'56"	162°	FL151	19 nmi
5	N44°22'17" E3°17'46"	N44°28'16" E3°43'33"	072°	FL151	19 nmi
6	N44°24'52" E3°39'08"	N44°11'08" E3°19'60"	225°	FL150	19 nmi
7	N44°12'59" E3°16'19"	N44°12'58" E3°43'20"	090°	FL151	19 nmi
8	N44°06'46" E3°37'12"	N44°20'29" E3°18'06"	315°	FL151	19 nmi
9	N44°26'23" E3°37'01"	N44°12'39" E3°17'53"	225°	FL150	19 nmi

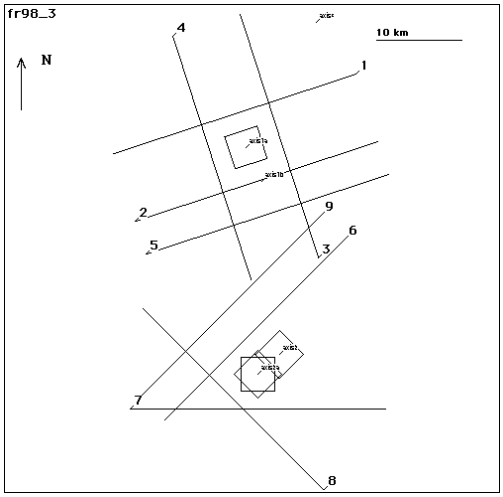

Figure 13. Flight plan for mission 3 on 18 May 1998.

Table 6. Flight plan May 19.

Pass	Begin	End	Heading	Alt	L
1	N44°34'39" E3°40'41"	N44°28'39" E3°14'51"	252°	FL151	19 nmi
2	N44°24'22" E3°16'49"	N44°30'22" E3°42'37"	072°	FL151	19 nmi
3	N44°20'59" E3°35'54"	N44°39'27" E3°27'32"	342°	FL151	19 nmi
4	N44°38'03" E3°21'32"	N44°19'35" E3°29'56"	162°	FL151	19 nmi
5	N44°22'17" E3°17'46"	N44°28'16" E3°43'33"	072°	FL151	19 nmi
6	N44°35'14" E3°38'48"	N44°17'38" E3°27'19"	205°	FL151	19 nmi
7	N44°20'15" E3°18'42"	N44°26'14" E3°44'28"	072°	FL151	19 nmi
8	N44°19'32" E3°21'37"	N44°37'09" E3°33'05"	025°	FL150	19 nmi
9	N44°46'22" E3°41'06"	N44°31'04" E3°24'20"	218°	FL151	19 nmi
10	N44°47'37" E3°38'51"	N44°32'19" E3°22'05"	218°	FL151	19 nmi

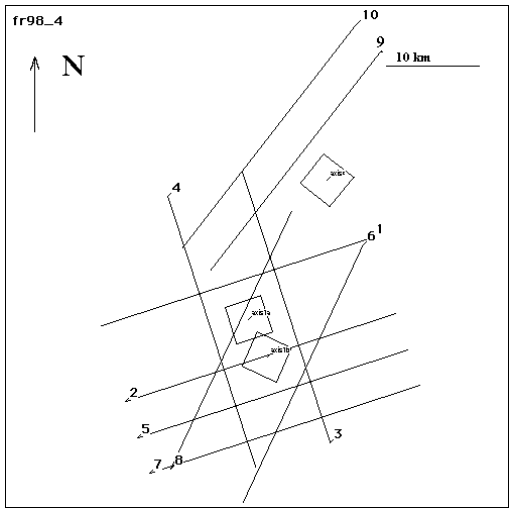

Figure 14. Flight plan for mission 4 on 19 May 1998.

4. SAR image generation

4.1 SAR processing

The radar data have been processed using the standard CARABAS SAR processor, i.e. including pulse compression, RFI filtering and azimuth compression (back-projection) as illustrated in Figure 15. Two versions of the backprojection algorithm have been used. The original "global" backprojection (GBP) algorithm, which performs direct time-domain integration for each pixel. The other algorithm is called "factorised" backprojection (FBP) which has been developed to reduce processing time without sacrificing image quality. It is a recursive algorithm, which splits the processing into a number of stages and generates images with successively finer resolution. Descriptions of the algorithms can be found in [8-9].

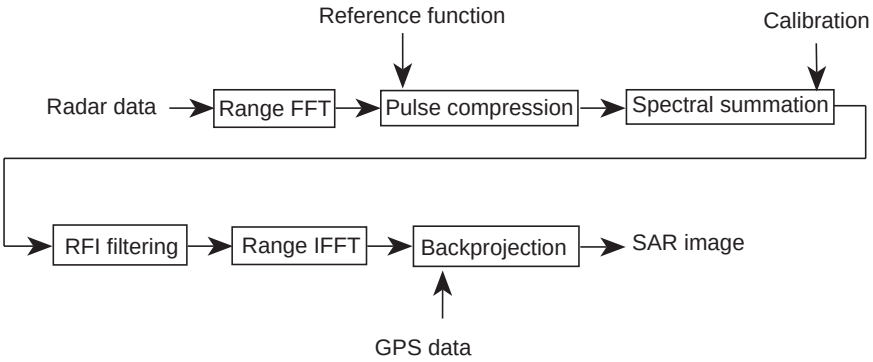

Figure 15. Block diagram of the CARABAS SAR processor.

A total of 73 CARABAS images have been processed and are summarised in Tables 7-10. Most have been processed with the "Fac" processor, which includes the GPB algorithm. A few have also recently been processed with the "Fbp" processor, which includes the FBP algorithm. The image file name can be used to uniquely identify the campaign, mission, pass and image version. For example, fr98_1_2_11 means campaign fr98, mission 1, pass 2 and image version 11. The image sizes given in the tables correspond to a pixel spacing of 1 m, whereas the aperture sizes correspond to an element spacing of about 0.9375 m. The last column indicates whether radiometric calibration has been performed on the imagery, which is also indicated by the full file name which then includes the letters "RFcorr". A total of 24 CARABAS images have been radiometrically calibrated in this way.

Table 7. Processed images from mission 1 in Les Landes.

Image name	Image size	Aperture size	Area	Processor	Calibration
fr98_1_1_15	2048 x 2048	8192	Nezer forest	Fac	Yes
fr98_1_1_18	2048 x 2048	8192	Nezer forest	Fbp	No
fr98_1_2_11	2048 x 2048	8192	Nezer forest	Fac	Yes
fr98_1_2_13	2048 x 2048	8192	Nezer forest	Fbp	No
fr98_1_3_5	2048 x 2048	8192	Nezer forest	Fac	Yes
fr98_1_3_7	2048 x 2048	8192	Nezer forest	Fbp	No
fr98_1_4_5	2048 x 2048	8192	Nezer forest	Fac	Yes
fr98_1_4_7	2048 x 2048	8192	Nezer forest	Fbp	No
fr98_1_5_3	2048 x 2048	8192	Nezer forest	Fac	Yes
fr98_1_5_5	2048 x 2048	8192	Nezer forest	Fbp	No
fr98_1_6_2	2048 x 2048	8192	Nezer forest	Fac	Yes
fr98_1_6_4	2048 x 2048	8192	Nezer forest	Fbp	No
fr98_1_7_8	2048 x 2048	8192	Nezer forest	Fac	Yes
fr98_1_7_12	2048 x 2048	8192	Nezer forest	Fbp	No
fr98_1_8_5	2048 x 2048	16384	Nezer forest	Fac	No
fr98_1_8_6	2048 x 2048	8192	Nezer forest	Fac	Yes
fr98_1_8_9	2048 x 2048	8192	Nezer forest	Fbp	No
fr98_1_9_12	2048 x 2048	8192	Nezer forest	Fac	Yes
fr98_1_9_15	2048 x 2048	8192	Nezer forest	Fbp	No
fr98_1_10_3	2048 x 2048	8192	Nezer forest	Fac	Yes
fr98_1_10_6	2048 x 2048	8192	Nezer forest	Fbp	No

Table 8. Processed images from mission 2 in Les Landes.

Image name	Image size	Aperture size	Area	Processor	Calibration
fr98_2_1_12	2048 x 2048	8192	Nezer forest	Fac	No
fr98_2_1_18	2048 x 2048	8192	Nezer forest	Fbp	Yes
fr98_2_2_6	2048 x 2048	8192	Nezer forest	Fac	No
fr98_2_2_9	2048 x 2048	8192	Nezer forest	Fbp	Yes
fr98_2_3_4	2048 x 2048	8192	Nezer forest	Fac	No
fr98_2_3_6	2048 x 2048	8192	Nezer forest	Fbp	Yes
fr98_2_4_3	2048 x 2048	8192	Nezer forest	Fac	No
fr98_2_4_6	2048 x 2048	8192	Nezer forest	Fbp	Yes
fr98_2_5_3	2048 x 2048	8192	Nezer forest	Fac	No
fr98_2_5_6	2048 x 2048	8192	Nezer forest	Fbp	Yes
fr98_2_6_3	2048 x 2048	8192	Nezer forest	Fac	No
fr98_2_6_5	2048 x 2048	8192	Nezer forest	Fbp	Yes
fr98_2_7_3	2048 x 2048	8192	Nezer forest	Fac	No
fr98_2_7_6	2048 x 2048	8192	Nezer forest	Fbp	Yes
fr98_2_8_3	2048 x 2048	8192	Nezer forest	Fac	No
fr98_2_8_7	2048 x 2048	8192	Nezer forest	Fbp	Yes
fr98_2_9_9	4096 x 5120	16384	Dune de Pyla	Fac	No
fr98_2_9_10	4096 x 5120	8192	Dune de Pyla	Fac	No
fr98_2_10_3	4096 x 5120	16384	Dune de Pyla	Fac	No
fr98_2_10_5	4096 x 5120	20224	Dune de Pyla	Fac	No

Table 9. Processed images from mission 3 in Lozère.

Image name	Image size	Aperture size	Area	Processor	Calibration
fr98_3_1_9	2048 x 2048	8192	Causse Mende forest	Fac	No
fr98_3_1_10	2048 x 2048	8192	Causse Mende targets	Fac	No
fr98_3_2_12	2048 x 2048	8192	Causse Mende forest	Fac	No
fr98_3_2_13	2048 x 2048	8192	Causse Mende targets	Fac	No
fr98_3_3_3	2048 x 2048	8192	Causse Mende forest	Fac	No
fr98_3_3_4	2048 x 2048	8192	Causse Mende targets	Fac	No
fr98_3_4_3	2048 x 2048	8192	Causse Mende forest	Fac	No
fr98_3_4_4	2048 x 2048	8192	Causse Mende targets	Fac	No
fr98_3_5_4	2048 x 2048	16384	Causse Mende targets	Fac	No
fr98_3_5_5	2048 x 2048	16384	Causse Mende forest	Fac	No
fr98_3_5_6	2500 x 5000	16384	Causse Mende	Fac	No
fr98_3_6_8	2048 x 2048	8192	Causse Mejean	Fac	No
fr98_3_7_4	2048 x 2048	16384	Causse Mejean	Fac	No
fr98_3_8_4	2048 x 2048	16384	Causse Mejean	Fac	No
fr98_3_9_3	2048 x 2048	16384	Causse Mejean	Fac	No

Table 10. Processed images from mission 4 in Lozère.

Image name	Image size	Aperture size	Area	Processor	Calibration
fr98_4_1_9	2048 x 2048	8192	Causse Mende forest	Fac	No
fr98_4_1_10	2048 x 2048	8192	Causse Mende targets	Fac	No
fr98_4_1_11	2500 x 5000	16384	Causse Mende	Fac	Yes
fr98_4_2_8	2048 x 2048	8192	Causse Mende forest	Fac	No
fr98_4_2_9	2048 x 2048	8192	Causse Mende targets	Fac	No
fr98_4_2_10	5000 x 5000	16384	Causse Mende	Fac	Yes
fr98_4_3_5	2048 x 2048	8192	Causse Mende forest	Fac	No
fr98_4_3_6	2048 x 2048	8192	Causse Mende targets	Fac	No
fr98_4_4_5	2048 x 2048	8192	Causse Mende forest	Fac	No
fr98_4_4_6	2048 x 2048	8192	Causse Mende targets	Fac	No
fr98_4_5_12	2500 x 5000	16384	Causse Mende	Fac	Yes
fr98_4_6_25	3250 x 3500	16384	Causse Sauveterre	Fac	Yes
fr98_4_6_26	3250 x 3500	16384	Causse Sauveterre	Fac	Yes
fr98_4_7_5	2500 x 5000	20000	Causse Mende	Fac	Yes
fr98_4_8_2	3250 x 3500	16384	Causse Sauveterre	Fac	No
fr98_4_9_2	3000 x 4096	16384	Lac de Charpal	Fac	No
fr98_4_9_3	2048 x 2048	8192	Lac de Charpal	Fac	No

4.2 SAR calibration procedure

The radiometric calibration of the CARABAS SAR images in this report is based on in-scene trihedrals with a (short) side length of 5.1 m. A detailed description of the methodology is described elsewhere [10]. In this section we only summarise the main steps involved.

The radar-cross section (RCS) of a trihedral on ground is computed using the FDTD (finite-difference time-domain) method. This is a numerical method, which discretises Maxwell's

equations and the scattering object in both space and time. The ground is modelled as a lossy dielectric half-space.

FDTD computes the complex scattering matrix over a bandwidth of 20-90 MHz and a Doppler cone angle of +/- 50° from the broadside direction. The scattering amplitudes are then combined to model the ideal SAR system response of the trihedral. Besides taking into account the mapping from transmit and Doppler frequency to across- and along-track frequency, a model of the polarisation response of the antenna is used.

The calibration process starts by extracting an image chip around the trihedral which is transformed to spectral domain using a 2D FFT. This response is compared to the ideal trihedral response and a correction function based on a second-order polynomial fit as a function of radial frequency is applied.

The corrected trihedral response is filtered to the selected frequency domain support, i.e. typically a bandwidth of 20-80 MHz and a Doppler cone angle of +/- 35° is used. The corresponding time-domain response is then obtained by a 2D IFFT. The calibration constant is determined as the ratio of the integrated response of the trihedral and the average RCS over the frequency-domain support. The integrated response is obtained by summation of the magnitude-squared pixel values over the trihedral response followed by subtraction of the estimated background level [11].

The image is radiometrically calibrated by filtering, scaling and finally applying a correction for the range-spreading loss. No correction is applied for the antenna gain pattern since measurements have shown this effect to be small within the normal swath.

The RCS (in m^2) of a pixel can be obtained by taking the magnitude and squaring the corresponding complex pixel value. The backscattering coefficient σ^o can also be determined by area averaging and scaling according to

$$\sigma^{o} = \frac{\cos\psi}{\delta_r \delta_a} \left\langle |DN|^2 \right\rangle - \sigma^{o}_{noise} \qquad (1)$$

where DN is the (complex) pixel value, δ_r and δ_a are the pixel spacings in slant range and azimuth, respectively, and $\cos\psi$ is the projection-cosine between slant and ground range [12].

A bug in the calibration software was corrected during the RAMCAR-98 analysis. The end result is that there is a small systematic difference of about 0.25 dB between measurements done during the early and late phases of the analysis. Most of the images have been calibrated with the original software, which results in overestimating the backscattering cross sections by 0.25 dB. The only exception is the images from mission 2 in Les Landes, which were recently calibrated. The difference of 0.25 dB is however quite small and can be neglected in comparison with other error sources.

5. Analysis of experimental data

5.1 Nezer forest, Les Landes

5.1.1 Experiment overview

The CARABAS SAR acquired radar data on 12 and 14 May 1998 over the Nezer forest in south-western France, just south of the city of Bordeaux. Data were collected during ten and eight flight tracks during the two days, respectively, and images have successfully been generated from all of them. Image quality (resolution and noise) varies slightly from image to image depending on the ability of the processor to remove RFI and antenna back-lobe effects. Radiometric calibration of images from all tracks has been performed in order to compute the RCS of targets as well as the backscattering coefficient of clutter and noise, respectively.

The Nezer mission included a target signature experiment, which is illustrated in Figures 16 and 17. A total of six vehicle targets were located in clear-cut and forested areas. Two 5-m large trihedral radar reflectors were also deployed by FOA for radiometric calibration and for measuring forest attenuation.

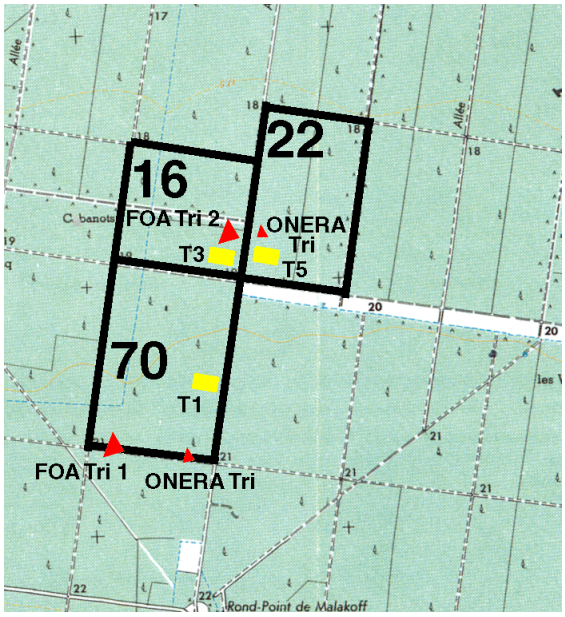

Figure 16. Deployment in Nezer forest on 12 May 1998. The positions of three vehicle targets (T1, T3 and T5), two FOA trihedrals Tri 1-2, and two ONERA trihedrals are shown.

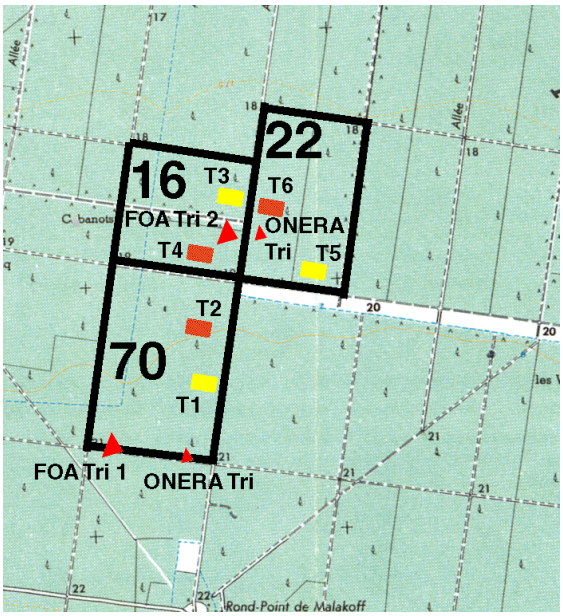

Figure 17. Deployment in Nezer forest on 14 May 1998. The positions of six vehicle targets T1-T6, two FOA trihedrals Tri 1-2, and two ONERA trihedrals are shown..

The vehicles are designated by T1 to T6. All vehicles were available during the second flight day, but only T1, T3 and T5 during the first flight day. The latter three were deployed in different configurations for the two days. The vehicles were always oriented pointing eastwards.

T1 and T2 were located in a clear-cut area in the open, whereas T3 and T4 were located in old forest (stand #16) which had been planted in 1952 or 1955. T5 and T6 were located in medium-aged forest (stand #22) which had been planted in 1980.

The forest consists of Maritime pine (*Pinus pinaster*) and is carefully managed to ensure homogeneous stands. Topography is perfectly flat and the ground surface is located close to sea level. A peculiarity of this test site is that most stands are planted along regular east-west lines, in general forming rows with 4-m spacing after thinning. The regular row spacing has been observed to result in Bragg-scattering resonance when illuminated perpendicular to the row direction [13]. This means that the radar gives a particularly high response for frequencies which fulfil the Bragg resonance condition.

FOA trihedral #1 was located on a gravel road in a clear-cut area with small bushes and a rather rough surface (rms height: 5-10 cm). The road was surrounded by ditches with a visible standing water. A car used for transportation of people and equipment was often parked on a nearby orthogonal road some hundred meters away. Trihedral #1 was rotated for each flight track so that its symmetry plane was always orthogonal to the flight track. Such an arrangement assures that the trihedral RCS is large and therefore useful for radiometric calibration. The deployment of trihedral #1 is illustrated in Figures 18-20.

Trihedral #2 was erected inside the old forest and always pointed westwards (magnetic bearing 272°). The deployment of trihedral #2 is illustrated in Figure 21.

Figure 18. Deployment of FOA trihedral #1: The first triangular panel is mounted together from three square and three triangular sections. The short side length is 5.1 m.

Figure 19. Deployment of FOA trihedral #1: The vertical panels are being mounted.

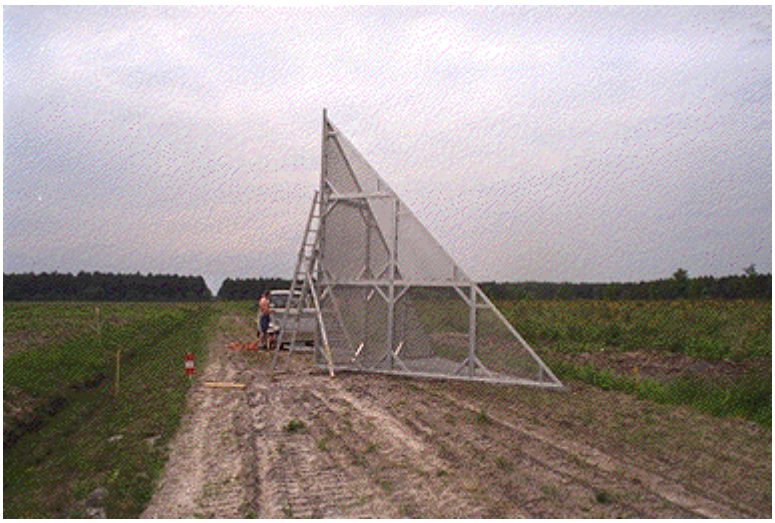

Figure 20. The deployment of FOA trihedral #1 is completed.

Figure 21. The deployment of FOA trihedral #2 inside forest stand #16.

ONERA also deployed two smaller (1.8 m) trihedral reflectors in the area. One was located further down the same gravel road as FOA trihedral #1, whereas the other was located in the medium-aged forest. Both reflectors were rotated to the radar line-of-sight.

Two examples of CARABAS images over the Nezer forest are shown in Figures 22-23. They correspond to the same flight pass 8 but acquired on 12 and 14 May, respectively. The bright areas correspond to old forests, and dark areas correspond to clear-cuts and roads. The targets and trihedrals are indicated by red squares and are all visible in the images. Note that the images are represented as slant range images and have not be projected to ground range. After ground range transformation and rotation, images can be matched and change images formed [14]. Two examples of change images are presented in Figure 24. The target-to-background ratio is now significantly enhanced which enables the targets to be easily detected. Note that the images in Figure 24 are sub-images from Figures 22-23. The pixel value in the change image represents the likelihood that a change has occurred [14].

The VHF-band signatures of targets and clutter have been analysed based on calibrated CARABAS images and is presented in the following sections. All targets could visually be identified in all images. This process is simplified by comparison with the image from the same pass but the other mission.

For each target, the RCS has been measured by integrating over the image response which has been judged to correspond to the target. Next, the background (clutter and noise) was characterised by its backscattering coefficient σ°, i.e. RCS normalised to ground area. Finally, the image noise level was estimated by computing the backscattering coefficient over a dark area nearby. The noise consists of both additive and multiplicative contributions and is unfortunately not constant over the image. Therefore, the estimated noise level is only a crude indication of the image noise level. In the next two sections, we show and discuss the clutter and target results, respectively.

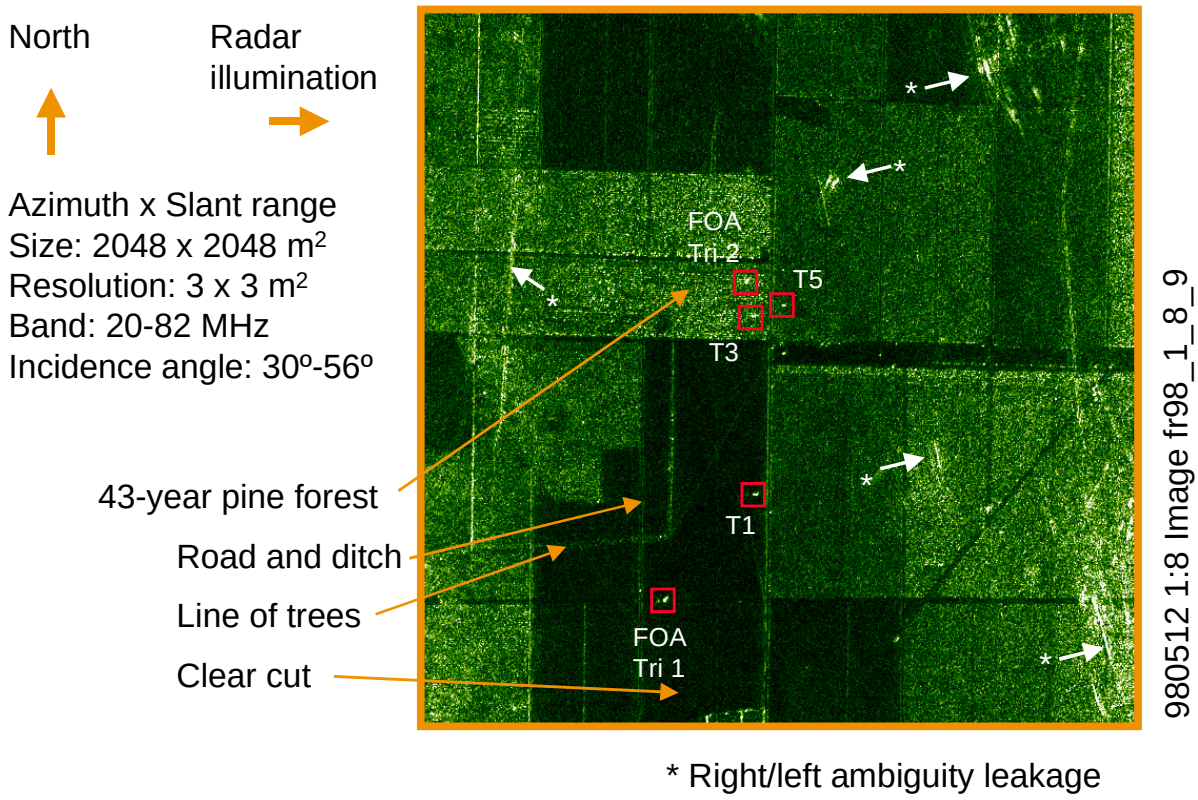

Figure 22. CARABAS image from Nezer forest in Les Landes acquired on 12 May 1998. The deployed targets and trihedrals are indicated by red squares.

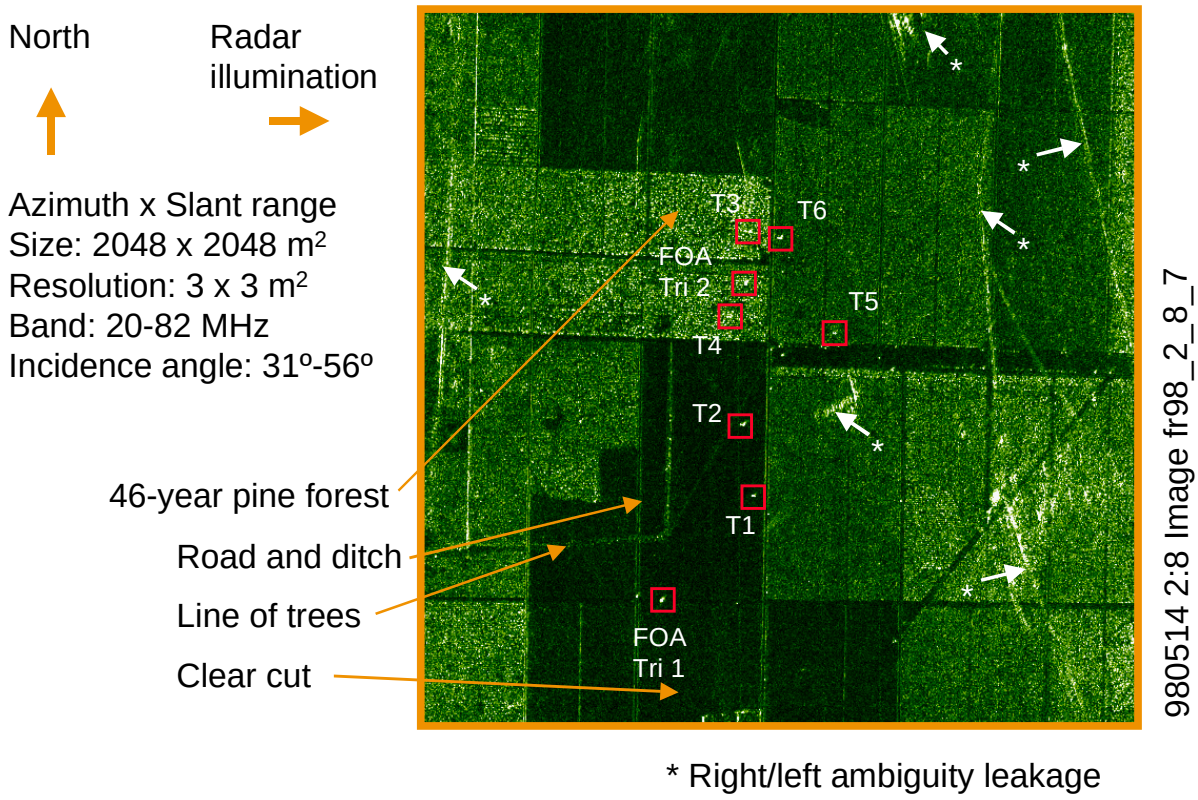

Figure 23. CARABAS image from Nezer forest in Les Landes acquired on 14 May 1998. The deployed targets and trihedrals are indicated by red squares.

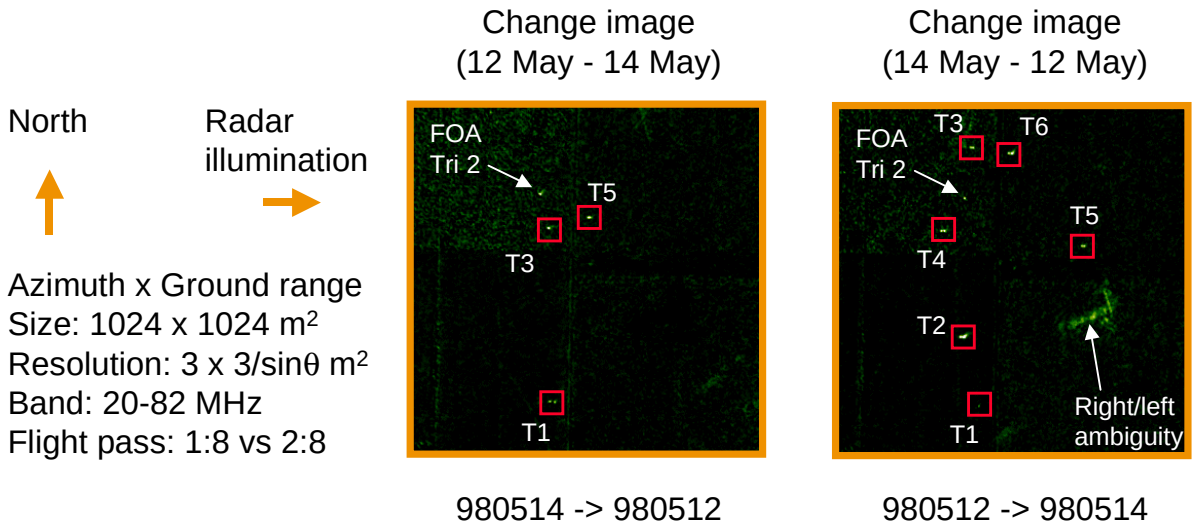

Figure 24. CARABAS change images derived from a sub-section of the images in Figures 22-23. The targets are enhanced relative the background level and can all be detected. The response from trihedral #2 and a right/left ambiguity is also visible in the change images.

5.1.2 Clutter analysis

A summary of all the backscatter measurements over the clear-cut and forested areas is given in Tables 11-12. The analysis has been performed on calibrated images with a bandwidth of 60 MHz (20-80 MHz) and a Doppler beamwidth of 70° (+/- 35° from zero Doppler) They have been ordered according to the flight heading, i.e. starting with the eastbound tracks and ending with the northbound tracks. Measurements from both flight days (missions) are included in the same table.

Four areas have been characterised, i.e. the clear-cut area where trihedral #1 was located, the medium-aged forest, and two areas of the old forest. Additionally, the image noise level has been estimated from the darkest area in each image.

We first note that the image noise floor varies considerably between the images, with an average value of –24 dB and a standard deviation of 2 dB. The noise floor varies in the range –20 dB to –27 dB for the different images. In general, the noise level is higher in images from mission 1 compared to mission 2. There are at least two reasons which explain this observation. Firstly, the transmitted waveform during mission 1 was not the intended one and the system was recalibrated before well-focused images could be produced. Nevertheless, the image quality is slightly worse for mission 1 due to residual and uncompensated errors. Secondly, the images from mission 1 were the first to be radiometrically calibrated and analysed. Later, when the images from mission 2 were going to be analysed improvements had been made to the processor which reduced the noise floor. The most significant improvement was a modified RFI filter which was used to generate new images from mission 2. The resulting difference can be seen in the average noise levels for mission 1 and 2, respectively. The average noise level is –23 dB for mission 1 and –26 dB for mission 2, i.e. a significant improvement of 3 dB.

Backscattering from bare ground surfaces is normally very low at VHF-band due to the long wavelengths which makes the surface roughness much smaller than the wavelength. Indeed, the clear-cut area in the images has a backscattering coefficient close to the image noise floor.

There are hardly any visible features in the clear-cut area for the images from mission 1, since the backscattering coefficient is only 1 dB above the noise level. However, in the improved images from mission 2 several prominent features, including diagonal ditches, are visible in the images. After subtraction of the noise power, the clear-cut area has an average backscattering coefficient of –26 dB.

The medium-aged forest (stand #22 with 18 years old trees) gave backscattering coefficients (noise not subtracted) in the range from –15 to –21 dB for the different images. Some of this variation is explained by the expected decrease with incidence angle, but also by a variable noise level. Most of the tracks had incidence angles in the range 43°-52° where the backscattering coefficient varied between –15 to –18 dB. Two of the tracks from mission 1, however, had an incidence angle around 65° and the backscattering coefficient was also lower in these cases, i.e. –20 and –21 dB, respectively. The average value for missions 1 and 2 are similar, although it was expected that the higher noise in the former case would have increased the values for mission 1. However, there may sometimes also be an effect of antenna backlobe leakage which introduces artifacts and increases the measured image intensity. For example, this is the main reason that the backscattering coefficient is 0.4 dB higher for 2:1 compared to 1:1, i.e. tracks with the same nominal incidence and heading but from different missions. After subtraction of the noise floor, the medium-aged forest has an average backscattering coefficient of –19 dB for mission 1 and –18 dB for mission 2. This difference is within the error tolerance due to the different incidence angles and variable noise level in the images.

The old forest (stand #16) was divided into two separate areas called S (south) and N (north). Stand #16 N was planted in 1952, whereas #16 S was planted in 1955. In practise, the two areas had very similar backscattering coefficients (noise not subtracted) varying in the range from –11 to –17 dB. Just as for the medium-aged forest, the two tracks with higher incidence angles gave a backscattering coefficient which was a few dB lower. After subtraction of the noise floor, the old forest areas gave a backscattering coefficient of about –13 dB.

In summary, the average backscattering coefficients measured for the open field, medium-aged forest and old forest were –26 dB, –18 dB, and –13 dB, respectively.

Table 11. Nezer clutter analysis: Mission 1 (12/5) and 2 (14/5) - *Noise not subtracted.*

Heading	Mission : Pass	Clear-cut area Stand #70		Maritime pine forest (1980) Stand #22		Maritime pine forest (1955) Stand #16 S		Maritime pine forest (1952) Stand #16 N		Image noise level
		θ (º)	σº (dB)	θ (º)	σº (dB)	θ (º)	σº (dB)	θ (º)	σº (dB)	σº (dB)
97º	1:1	50,3	-21,6	44,4	-16,4	45,8	-12,6	43,3	-10,9	-22,4
	2:1	49,3	-23,9	43,1	-16,0	44,4	-12,6	42,0	-11,3	-27,1
127º	1:3	50,0	-19,0	44,2	-17,4	47,2	-13,0	45,2	-12,1	-22,2
	2:3	52,4	-22,1	44,0	-17,7	47,5	-12,5	45,5	-12,0	-26,6
157º	1:5	51,0	-20,3	44,4	-16,7	49,2	-12,2	47,6	-11,5	-20,5
	2:5	50,2	-21,0	43,4	-16,7	48,3	-11,9	47,0	-11,4	-23,7
187º	1:7	50,9	-20,4	46,8	-15,5	51,1	-11,8	50,7	-11,7	-20,7
	2:7	50,1	-24,7	45,7	-15,3	50,3	-11,6	50,2	-11,7	-26,3
277º	1:2	44,1	-21,4	51,4	-17,7	49,9	-14,3	51,8	-14,0	-23,3
	2:2	44,4	-23,6	50,9	-18,5	49,6	-14,6	51,4	-14,7	-27,2
	1:9	65,2	-25,1	66,9	-20,9	66,6	-16,6	67,3	-16,8	-25,7
307º	1:4	44,2	-19,7	51,7	-18,0	48,9	-13,1	50,8	-13,0	-22,9
	2:4	42,7	-20,0	50,7	-18,2	47,4	-11,9	49,4	-12,1	-25,3
337º	1:6	44,1	-18,9	50,7	-15,7	46,5	-10,7	48,1	-10,6	-19,9
	2:6	43,9	-23,6	51,3	-18,1	46,9	-12,0	47,9	-12,1	-25,7
007º	1:8	45,3	-21,4	49,5	-16,6	44,9	-11,3	44,7	-11,4	-21,6
	2:8	45,1	-24,7	49,7	-17,5	44,6	-12,0	44,7	-12,2	-25,7
	1:10	65,6	-25,7	67,2	-19,8	65,6	-16,2	65,8	-15,7	-26,5
Average	1 + 2		**-22,1**		**-17,4**		**-12,8**		**-12,5**	**-24,1**
RMS	1 + 2		2,2		1,5		1,6		1,7	2,4
Average	1		**-21,4**		**-17,5**		**-13,2**		**-12,8**	**-22,6**
RMS	1		2,3		1,7		2,0		2,1	2,2
Average	2		**-23,0**		**-17,3**		**-12,4**		**-12,2**	**-26,0**
RMS	2		1,7		1,1		1,0		1,1	1,1

Table 12. Mission 1 and 2: Average backscattering coefficients - *After noise subtraction.*

Heading	Mission : Pass	Clear-cut area Stand #70		Maritime pine forest (1980) Stand #22		Maritime pine forest (1955) Stand #16 S		Maritime pine forest (1952) Stand #16 N	
		θ (º)	σº (dB)	θ (º)	σº (dB)	θ (º)	σº (dB)	θ (º)	σº (dB)
Average	1 + 2	49	**-26**	50	**-18**	50	**-13**	50	**-13**
Average	1	51	**-28**	52	**-19**	52	**-14**	52	**-13**
Average	2	47	**-26**	47	**-18**	47	**-13**	47	**-12**

5.1.3 Target analysis

The RCS measurements of all six vehicle targets (T1-T6) are summarised in Table 13. The same images have been used as in the previous section, i.e. the calibrated images have a bandwidth of 60 MHz (20-80 MHz) and a Doppler beamwidth of 70° (+/- 35° from zero Doppler).

The measurements consist of the total RCS of the target, i.e. the integrated RCS over the image features judged to originate from the target. This method introduces some extra uncertainty due to its subjective nature. An alternative would have been to measure the peak value, i.e. the RCS of the dominating resolution cell. The problem with the latter, however, is that peak measurements are notoriously sensitive to focus errors and thus more difficult to interpret. The total RCS is also useful since it indicates the potential of incoherent integration over a number of resolution cells in order to improve the detection performance.

Targets T1, T3 and T5 are of the same type but located in different backgrounds. T1 was located in approximately the same position for both mission, whereas T3 and T5 were moved within the same forest stand. T1 was located on the clear-cut field and has a measured RCS in the range 14 – 20 dBm^2 with an average value of 17.2 dBm^2. The RCS variation of T3 is 13 – 20 dBm^2 and with a slightly lower average value of 16.4 dBm^2, i.e. 0.8 dB lower than T1. This is a quite small difference considering that T3 was located in the old forested areas (stand #16). For T5 which was located in the medium-aged forest (stand # 22), the RCS shows a larger variability in the range 7 – 18 dBm^2 with an average of 14.4 dBm^2. The medium-aged forest therefore seems to give more attenuation than the old forest, i.e. the RCS is about 3 dB lower than T1, but also a greater RCS variability.

The interpretation of these results may first seem confusing since the medium-aged forest stand gave an average RCS reduction of 2.8 dB compared to 0.8 dB for the old forest. However, it is recognised that the attenuation in a forest canopy is normally not dominated by scattering losses due to the trunks but rather from the water content in the canopy layer. The number of trunks per unit area in older stands normally decreases whereas the average trunk volume increases as well as the stand volume. However, the amount of canopy biomass per trunk is essentially constant implying that the biomass of the canopy layer per unit area actually decreases and therefore also the attenuation. For more information on the attenuation measurements, see section 5.1.4.

T2, T4 and T6 are also of the same target type but located in different backgrounds. These targets were only available for mission 2. The results are this time slightly different, i.e. both targets T4 and T6 standing in the forested areas gave a RCS which, on average, is about 2 dB lower than target T2 in the clear-cut area. The RCS of T2 varies in the range 14-18 dBm^2 with an average value of 16.4 dBm^2. The RCS of T4 and T6 varies in the range 12-17 dBm^2 with an average value of 14.7 dBm^2 and 14.5 dBm^2, respectively.

In summary, the target RCS varied in the range 7-20 dBm^2. The lowest measurement 7 dBm^2 was, as expected, observed for the largest incidence angles (67°) and in the forest. The reason was presumably multi-path interference from the ground surface and forest attenuation. A significant variation with aspect angle was also observed. The highest RCS was generally observed when the flight track heading was east or west, i.e. when the radar illumination was broadside on the target.

Table 13. Nezer target analysis: Mission 1 (12/5) and 2 (14/5).

Heading	Mission : Pass	T1		T2		T3		T4		T5		T6	
		θ deg	σ dBm^2	θ deg	σ dBm^2	θ deg	σ dBm^2	θ deg	σ dBm^2	θ deg	σ dBm^2	θ deg	σ dBm^2
97º	1:1	50	20,1			46	19,4			46	17,9		
	2:1	49	18,7	47	17,7	42	20,0	45	14,9	45	17,3	42	15,2
127º	1:3	50	17,4			47	15,6			46	13,8		
	2:3	50	16,2	49	15,8	45	16,3	47	14,5	45	13,4	46	16,8
157º	1:5	50	15,3			48	14,2			47	15,0		
	2:5	49	14,3	49	14,6	46	15,4	48	13,4	45	10,3	45	11,9
187º	1:7	50	19,4			50	12,6			49	16,2		
	2:7	49	17,7	49	18,5	49	13,8	50	17,5	46	14,2	48	16,1
277º	1:2	45	18,8			50	18,2			50	16,8		
	2:2	45	18,6	47	15,8	51	18,7	49	14,8	49	16,2	51	12,5
	1:9	65	14,9			66	16,5			67	7,2		
307º	1:4	46	18,0			49	16,6			50	13,5		
	2:4	44	17,3	46	16,8	50	16,1	48	12,9	49	15,9	50	13,2
337º	1:6	46	15,5			48	15,0			49	13,8		
	2:6	46	15,8	46	14,4	49	15,2	47	12,9	50	12,6	50	13,3
007º	1:8	46	17,5			46	16,6			48	16,7		
	2:8	47	18,3	46	17,7	47	18,1	46	16,3	49	16,2	48	16,6
	1:10	66	16,0			66	16,5			66	11,4		
Average	1 + 2		**17,2**		**16,4**		**16,4**		**14,7**		**14,4**		**14,5**
RMS	1 + 2		1,7		1,5		2,0		1,6		2,7		2,0
Average	1		**17,3**				**16,1**				**14,2**		
RMS	1		1,8				1,9				3,1		
Average	2		**17,1**		**16,4**		**16,7**		**14,7**		**14,5**		**14,5**
RMS	2		1,6		1,5		2,1		1,6		2,3		2,0

5.1.4 Trihedral analysis

The RCS measurements of the two trihedrals are summarised in Table 14. The same images have been used as in the previous sections but limited to the heading with maximum RCS of FOA trihedral #2.

Table 14. Mission 1 and 2: RCS of FOA trihedrals.

Heading	Mission: Pass	FOA Tri 1 (clear-cut area)			FOA Tri 2 (stand #16 S)		
		θ	σ	σ_{theory}	θ	σ	
		deg	dBm^2	dBm^2	deg	dBm^2	
7°	1:8	43,2	**21,3**	21,3	46,3	**18,5**	
7°	1:10	65,0	**23,8**	23,7	66,0	**22,3**	
7°	2:8	43,5	**21,3**	21,3	46,5	**19,6**	

.

Trihedral T1 has been used for radiometric calibration of the images. Hence the small difference (max. 0.1 dB) obtained between RCS measurement and theory. The trihedrals may also be used to estimate the two-way attenuation induced by the forest. The attenuation varies in the range 1-3 dB and the results are shown in Table 15.

Table 15. Mission 1 and 2: Forest attenuation measurements.

Heading	Mission: Pass	FOA Tri 2 – Tri 1 (stand #16 S)	
		θ (average)	Attenuation
		(°)	(dB)
7°	1:8	45	**2.8**
7°	1:10	66	**1.5**
7°	2:8	45	**1.7**

5.2 Causse Mende, Lozère

5.2.1 Experiment overview

After completing the Les Landes missions described in Section 5.1, the CARABAS SAR was transferred to Marseille (Istres air base) and two flight missions were conducted in the mountainous Lozère Département. A typical view of the landscape is shown in Figure 25.

Data collection was performed on 18 and 19 May 1998 with nine flight tracks per day over three different areas: Causse Mende, Florac (Mejean), and Lac de Charpal.

Figure 25. View showing the general landscape on Causse Mende, Lozère Département. The forest grows on the undulating plateau at an altitude of 1000-1100 m. Deep canyons and gorges cut through the landscape down to an altitude of 700-800 m.

On 18 May, five tracks were flown over Causse Mende as well as four tracks over Florac with varying incidence and aspect angles. On 19 May, eight tracks were flown over Causse Mende and one track over Lac de Charpal.

The main area of interest was Causse Mende which included a target deployment and two extra trihedral sites as illustrated in Figure 26. The forests consist mainly of Austrian pine. A total of three vehicle targets were located in clear-cut and forested areas as shown in Figure 27. Four 5-m large trihedrals were also deployed by FOA for calibration purposes, of

which two were in the target experiment area (T1 and T2). One additional trihedral was located at the air field (T3) and one inside a forest in between (T4).

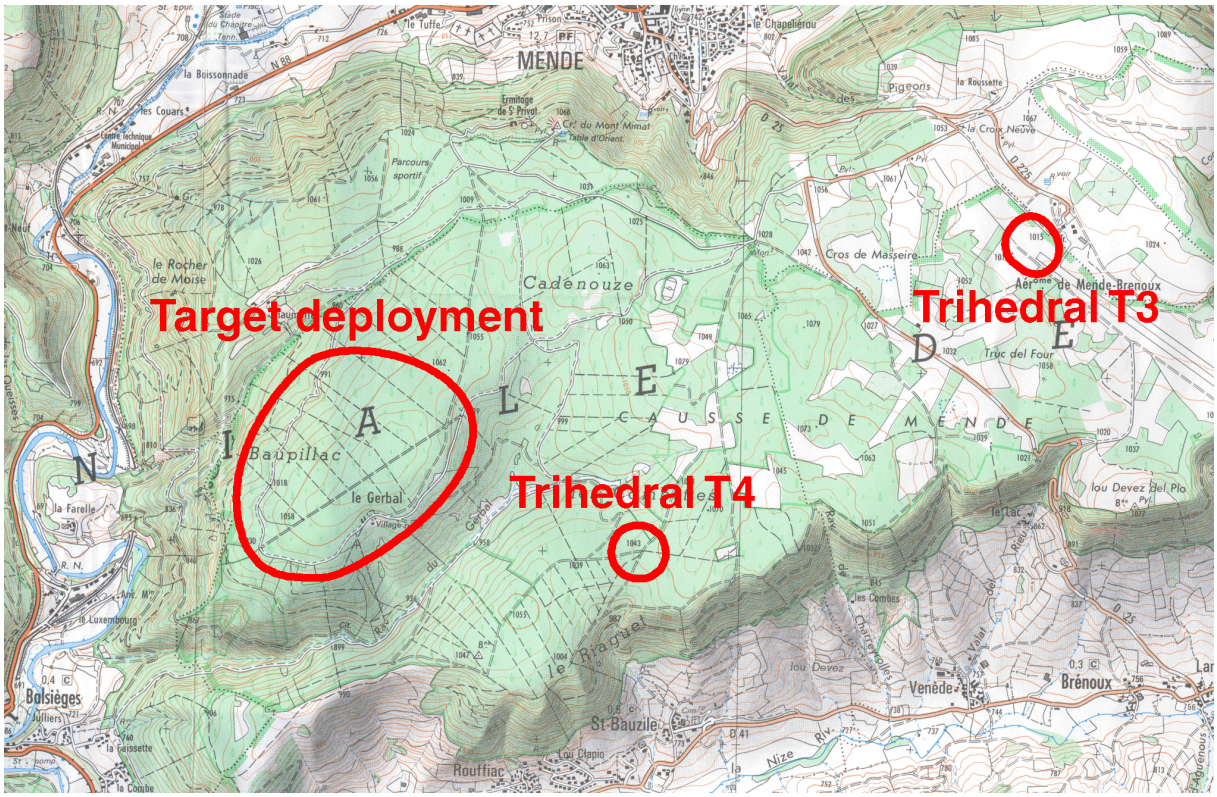

Figure 26. Map of the Causse Mende area including the main target deployment area (see Figure 27 for details) and the two trihedral sites T3 and T4.

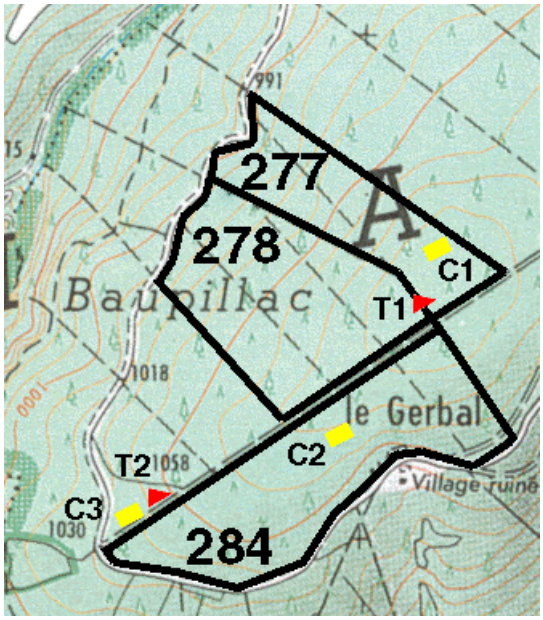

Figure 27. Target deployment in Causse Mende forest on 19 May 1998. Three vehicle targets C1-C3, and two FOA trihedrals T1-2 were deployed. The latter were also in place on 18 May 1998.

The three vehicles are designated by C1 to C3. The vehicles were only available during the second mission in Lozère (mission 4) and were oriented pointing south-west. C1 was located in dense forest (stand #277) pointing in magnetic bearing 240° and C2 in medium-dense forest (stand #284) with magnetic bearing 228°. Finally, C3 was located in a clear-cut area close to a road with magnetic bearing 238°.

The four trihedrals are designated by FOA-T1 to -T4. Figures 28-31 shows the deployed trihedrals. T1 was located in dense forest along a narrow clearing between stands #277 and #278, whereas T2 was located in the clear-cut area close to vehicle C3. Both of these trihedrals were oriented pointing approximately south-east (magnetic bearing 150°). Trihedral T3 was located on a grass field within the local airport area. This trihedral was rotated for each flight track so that its symmetry plane was always orthogonal to the flight track. The final trihedral T4 was located in a dense forest in between the vehicle target area and the airport area (between stands #309 and #310). T4 was pointed in nominally the same direction as T1 and T2.

Figure 28. Trihedral FOA-T1 deployed along narrow clearing between stands #277 and #278.

Figure 29. Trihedral FOA-T2 deployed in a clear-cut area.

Figure 30. Trihedral FOA-T3 deployed on the grass close to the airfield.

Figure 31. Trihedral FOA-T4 deployed between stands #309 and #310.

The signature analysis has concentrated on the vehicle target area. All possible images have been processed but only four have been radiometrically calibrated and analysed due to limited time. The four images are all from mission 4 when the vehicles were deployed and correspond to parallel but offset tracks. In this way, the effect of changing incidence angle could be assessed. One of the analysed images was acquired from a track located north of the target area, whereas the other three are from tracks located south thereof. Incidence angles therefore varied between 44° and 73°.

Two examples of CARABAS images over the Causse Mende forest are shown in Figure 32. They correspond to the same flight pass but acquired on 18 and 19 May, respectively. The bright areas correspond to old forests, and dark areas correspond to clear-cuts and roads. The targets and trihedrals are indicated by red squares and are all visible in the images. A change image is also shown to the right [14]. The target-to-background ratio is now significantly enhanced which enables the targets to be easily detected.

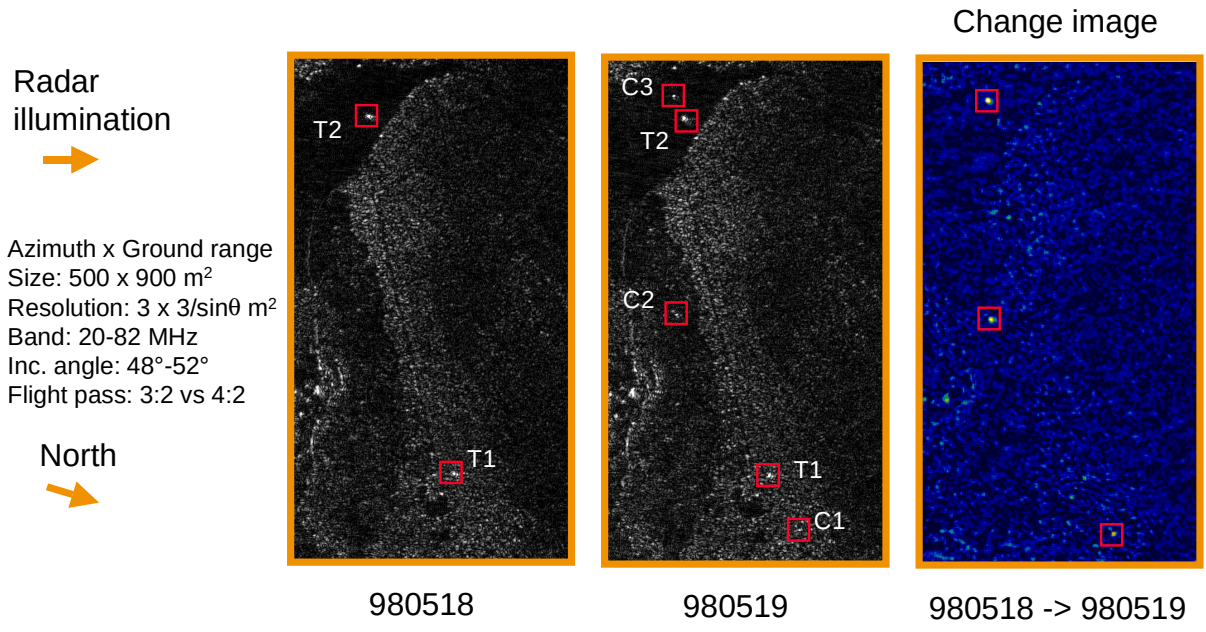

Figure 32. CARABAS image from Causse Mende forest in Lozère Département acquired on 18 and 19 May 1998. The deployed targets and trihedrals are indicated by red squares. A change image is also shown on the right. The targets are enhanced relative the background level and can all be detected.

The VHF-band signatures of targets and clutter are presented in the following sections. The analysis has only been performed on calibrated images of the targets, i.e. passes 1, 2, 5, and 7 from mission 4. All targets could visually be identified in all images. Only in one case was the target signature so weak that it was difficult to identify, i.e. target C1 in the image from mission 4 pass 7.

For each target, the RCS has been measured by integrating over the image response which has been judged to correspond to the target. Next, the background (clutter and noise) was characterised by its backscattering coefficient σ°, i.e. RCS normalised to ground area. Finally, the image noise level was estimated by computing the backscattering coefficient over a dark area nearby. The noise consists of both additive and multiplicative contributions and is unfortunately not constant over the image. Therefore, the estimated noise level is only a crude indication of the image noise level. In the next two sections, we show and discuss the clutter and target results, respectively.

5.2.2 Clutter analysis

A summary of all the backscatter measurements over the clear-cut and forested areas is given in Tables 16-17. The analysis has been performed on calibrated images with a bandwidth of 60 MHz (20-80 MHz) and a Doppler beamwidth of 70° (+/- 35° from zero Doppler).

Three clutter areas have been characterised, i.e. the clear-cut area with C3 and T2, the dense forest (stand #277/278) with C1 and T1, and the medium-dense forest (stand #284) with C2. Additionally, the image noise level has been estimated from a nearby dark area.

We first note that the image noise level is generally higher but more stable than in the Les Landes images. One reason is that the images have been processed with the original RFI filter which resulted in 3 dB higher noise level in the Les Landes images from mission 1 compared

to mission 2. The average noise level in Table 16 is then only about 1 dB higher compared to the Les Landes images with the same RFI filter. Another reason could be integrated sidelobe noise originating from strong scatterers located around the plateau rim.

The clear-cut area has an average backscattering coefficient of –19.4 dB without noise subtraction, which is 1.8 dB above the average noise level. After noise subtraction this results in a backscattering coefficient of about –24 dB, although the error may be quite large in this estimate since the clutter-to-noise ratio is rather poor. This backscattering coefficient is 2 dB higher compared to the clear-cut area measured in Les Landes.

The average backscattering coefficient after noise subtraction of the dense forest (stand #277/278) is –12 dB, whereas the medium-dense forest gave –19 dB. The range of variation is only 2 dB although the incidence angle changes significantly and two aspect angles are used. These results suggest that the stands are essentially on horizontal ground.

Table 16. Causse Mende clutter analysis: Mission 4 (19/5) - *Noise not subtracted.*

Heading	Mission : Pass	Clear-cut area		Austrian pine forest Stand #277/278		Austrian pine forest Stand #284		Image noise level
		θ (º)	σº (dB)	θ (º)	σº (dB)	θ (º)	σº (dB)	σº (dB)
252°	4:1	47	-18,2	44	-12,5	46	-17,1	-21,3
72°	4:2	48	-19,2	49	-10,8	48	-15,7	-21,7
72°	4:5	66	-19,4	66	-11,3	66	-17,7	-20,1
72°	4:7	73	-20,8	73	-11,6	73	-16,6	-21,6
Average	4		**-19,4**		**-11,6**		**-16,8**	**-21,2**
RMS	4		1,1		0,7		0,8	0,7

Table 17. Mission 4: Average backscattering coefficients - *After noise subtraction.*

Heading	Mission : Pass	Clear-cut area		Austrian pine forest Stand #277/278		Austrian pine forest Stand #284	
		θ (º)	σº (dB)	θ (º)	σº (dB)	θ (º)	σº (dB)
Average	4		**-24**		**-12**		**-19**

5.2.3 Target analysis

The RCS measurements of all three vehicle targets (C1-C3) are summarised in Table 18. The same images have been used as in the previous section.

Targets C1-C3 are all of the same type with similar orientation but located in different clutter backgrounds. In general, the highest RCS is found for C3 which was located in the clear-cut area. C3 gives similar RCS for passes 1 and 2 which have nearly the same incidence angle but 180° different aspect angle. The RCS of C3 decreases with increasing incidence angle, and at 73° it has been reduced by about 10 dB compared to the steeper incidence angles. Similar trends are noted for the concealed vehicles targets, except that C2 shows a significant difference between pass 1 and 2. The reason for this observation is presently not understood. The lowest RCS of 1 dBm^2 is found for C3 at highest incidence angle. Due to the low RCS it was difficult to measure with good confidence.

Table 18. Mission 4: Analysis of vehicle targets at Causse Mende.

Heading	Mission : Pass	C1 (stand #277)		C2 (stand #284)		C3 (clear-cut)	
		θ deg	σ dBm^2	θ deg	σ dBm^2	θ deg	σ dBm^2
252°	4:1	44	**10,6**	46	**8,9**	47	**14,8**
72°	4:2	49	**12,6**	48	**15,8**	48	**15,4**
72°	4:5	66	**5,5**	66	**7,7**	66	**11,1**
72°	4:7	73	**1,1**	73	**4,8**	73	**5,5**
Average	4		**7,4**		**9,3**		**11,7**
RMS			5,2		4,7		4,5

5.2.4 Trihedral analysis

The RCS measurements of all four trihedrals (T1-T4) are summarised in Table 19. The same images have been used as in the previous sections but with pass 1 excluded since it illuminated the rear of all trihedrals except T3. Trihedrals T2 (clear-cut area) and T3 (deployed at the airport) has been used for radiometric calibration of the images. Hence the small difference (max. 0.3 dB) obtained between RCS measurement and theory. T2 and T3 should have similar RCS for each track since both were deployed in the open and approximately at the same incidence angle. The measured average and rms difference is 0.6 dB and 0.5 dB, respectively, which confirms that the radiometric stability is about 1 dB.

Table 19. Mission 4: RCS of FOA trihedrals.

Heading	Mission: Pass	FOA T1 (stands #277/278)			FOA T2 (clear-cut area)			FOA T3 (air field)			FOA T4 (stands #309/310)		
		θ	σ		θ	σ	σ_{theory}	θ	σ	σ_{theory}	θ	σ	
		deg	dBm^2		deg	dBm^2	dBm^2	deg	dBm^2	dBm^2	deg	dBm^2	
72°	4:2	49	**19.7**		48	**21.9**	22.2	50	**22.5**	22.2	42	**21.0**	
72°	4:5	66	**22.3**		66	**24.0**	23.8	67	**23.9**	23.8	64	**23.0**	
72°	4:7	73	**20.5**		73	**23.4**	23.3	73	**24.5**	23.3	72	**21.6**	

.

The trihedral data may also be used to estimate the two-way attenuation induced by the forest. Most accurate measurements are obtained by comparing the measured RCS of trihedrals deployed nearby each other. We therefore compare T1 vs. T2 as well as T4 vs. T3. The forest attenuation is estimated from the RCS difference in dB. Calibration errors tend to cancel each other due to the subtraction operation, and we estimate that the attenuation measurement is accurate to within 0.5 dB. The results are shown in Table 20. The attenuation varies in the range 1-3 dB, with the highest value obtained for the highest incidence angle.

Table 20. Mission 4: Forest attenuation measurements.

Heading	Mission : Pass	FOA T2 – T1 (stands #277/278)		FOA T3 – T4 (stands #309/310)	
		θ (average)	Attenuation	θ	Attenuation
		(°)	(dB)	(°)	(dB)
72°	4:2	49	**2.2**	42	**1.5**
72°	4:5	66	**1.7**	64	**0.9**
72°	4:7	73	**2.9**	72	**2.9**

6. Dune du Pyla

On the Atlantic shoreline in the vicinity of the Nezer forest is the highest dune in Europe found, Dune du Pyla, see Figure 33. It has a height of 117 m. Photos of this spectacular natural formation can be found in Figures 34. The area was included to be imaged in the RAMCAR-98 experiment planning. The main objective was to co-register a comprehensive data set at several radar bands and investigate the possibility of ground penetration. The result from the image generation of one of the two CARABAS imaging passes (= 10) is found in Figure 35. A more detailed analysis of all the acquired radar data with respect to ground penetration will be carried out by other research groups who have access to good ground truth of the imaged area, e.g. the Astonomic Laboratory of Bordeaux University.

Figure 33. Map showing the Atlantic coast south of the town Arcachon. The Dune du Pyla, which can be found along the coastline, was imaged by the CARABAS SAR on 14 May 1998. Part of the Cazaux air base, used during the Les Landes missions, can be seen at the bottom right.

Figures 34. Three views of the Dune du Pyla along the Atlantic coast south of Arcachon. The view on the upper left shows sand banks which become visible during low tidal conditions.

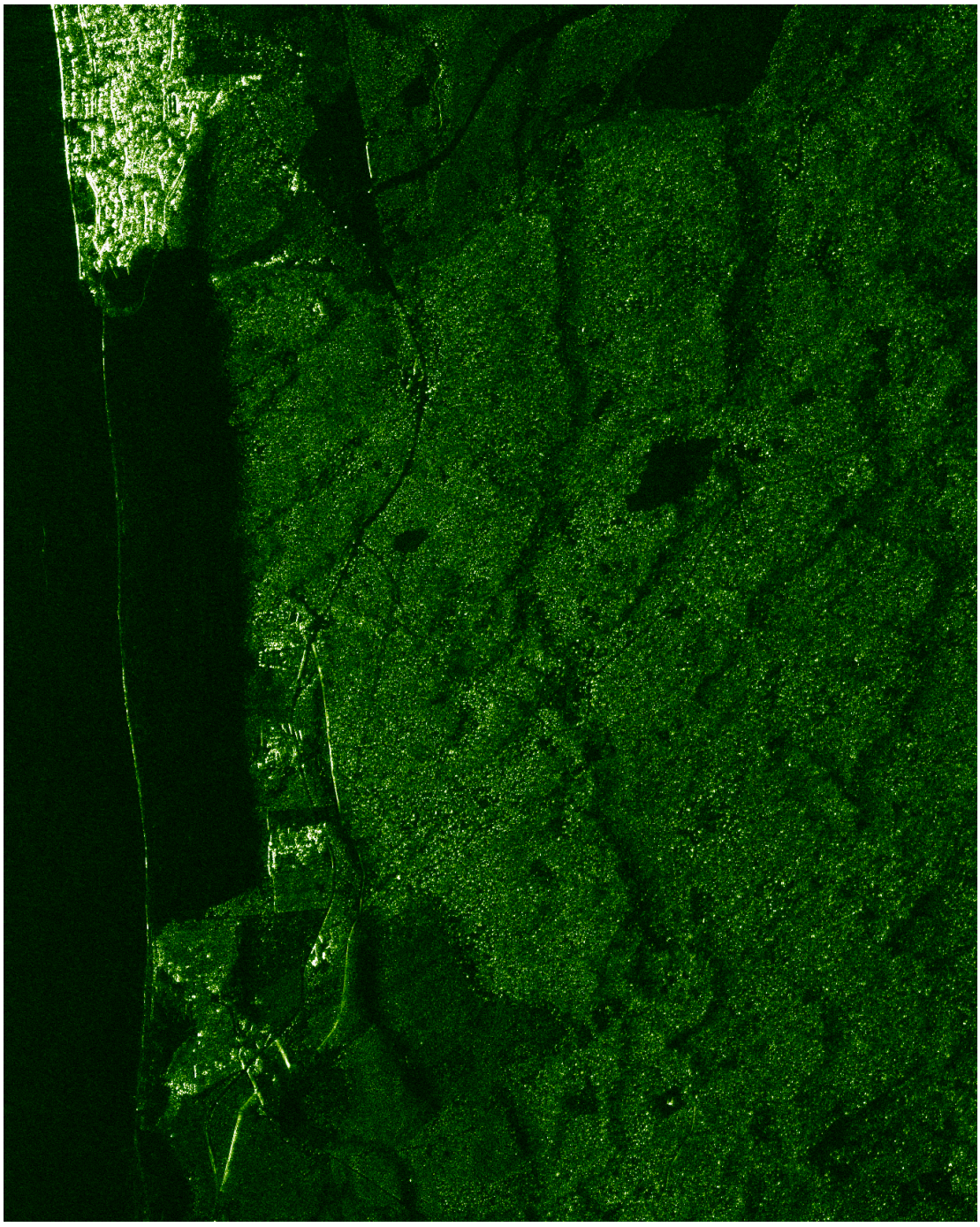

Figure 35. CARABAS image of the area surrounding Dune du Pyla. The image is represented in slant range and has a size of 5120 m x 4096 m with the radar illumination from the left. The flight altitude was 3150 m and the minimum range in the image is 6962 m. The processed aperture and bandwidth is 19 km and 22-82 MHz, respectively. The Atlantic ocean and the Dune du Pyla on the left side are both dark, but the coastline is visible as a bright narrow line. No visible structures are observed within the Dune. Forests expand to the right in the image and urban areas are visible as bright areas with linear structures mainly north (above) of the Dune. Some roads show up as dark curved features due to the absence of trees.

7. Conclusions

Four missions during RAMCAR-98 with image collections were conducted with CARABAS over test sites located in Les Landes and Lozère. SAR images from all flight tracks have successfully been processed. 73 images have been generated of which 24 have been radiometrically calibrated to an accuracy of ±1 dB. The radiometric calibration is based on measuring the response of in-scene trihedrals with known RCS. Measurements of radar-cross section (RCS) in m^2 are easily made from the latter images by simply taking the magnitude and squaring the complex pixel values.

Image quality, i.e. spatial resolution and noise, varies slightly from image to image. The main problems were encountered due to antenna back-lobe leakage which produces slightly defocused ambiguities from the opposite side of the flight track. The image quality is also dependent on the success of removing radio-frequency interference from the radar signal. Recent changes in the RFI filtering process reduced the noise level by about 3 dB.

The RCS of the vehicle targets were measured for different aspect and incidence angles. All RCS measurements varied in the range 1-20 dBm^2, with the smallest values observed for vehicles in forest concealment and for the largest incidence angle. These results are due to the combined effect of ground reflection interference and attenuation from the forest. For intermediate incidence angles (40-50°), the typical RCS of the vehicle targets was about 15 dBm^2 in the open and a few dB lower in the forest. For the largest incidence angles (73°), however, the RCS of the vehicle targets dropped down to 1-5 dBm^2.

The RCS of the vehicles also shows a variation with aspect angle. In Les Landes, the vehicles deployed in the open gave a RCS variation of 6 dB whereas the RCS variation of the vehicles in the forest were 13 dB. In Lozère, the RCS variation of the vehicles deployed in the open and in the forest was 10 dB and 15 dB, respectively.

Trihedrals were deployed inside three dense forest stands which enabled the forest attenuation to be assessed. The measured (two-way) attenuation varied between 0.9 and 2.9 dB. The maximum attenuation occurred for the largest incidence angle of 73°, but almost the same value of 2.8 dB was measured at 45° in one case.

Change detection has been applied to one image pair from each of the two areas. This method has been developed to detect both open and concealed vehicle targets. All targets were detected with only a few false alarms. The main problems arise due to artifacts caused by back-lobe leakage problems.

The VHF-band backscattering from forests is mainly related to stem volume, i.e. the volume of trunks per unit area. The CARABAS images also show that forest backscattering is sensitive to surface topography, i.e. surface gradient in both aspect and slope. The highest backscattering coefficient measured was –12 dB from old and dense forest, whereas the lowest backscattering coefficient of –28 dB was measured in a clear-cut area.

Two flight tracks over Dune du Pyla was also conducted. The SAR images, however, showed no evidence of sub-surface scattering presumably due to the high water content in the sand.

Additional results from RAMCAR-98 have also been reported in [15-18].

References

[1] Hellsten, H., Ulander, L.M.H., Gustavsson, A., and B. Larsson, Development of VHF CARABAS II SAR, Proc. Radar Sensor Technology, SPIE AeroSense Conference, Orlando, FL, 8-9 April 1996, SPIE vol. 2747, pp. 48-60, 1996

[2] Larsson, B., Frölind, P.-O., Gustavsson, A., Hellsten, H., Jonsson, T., Stenström, G., and L.M.H. Ulander, Some Results from the New CARABAS II VHF SAR System, Proc. Third International Airborne Remote Sensing Conference, Copenhagen, Denmark, 7-10 July 1997, pp. 25-32, 1997

[3] Ulander, L.M.H., and H. Hellsten, System Analysis of Ultra-Wideband VHF SAR, Proc. RADAR 97, Edinburgh, UK, 14-16 October 1997, pp. 104-108, 1997

[4] Gustavsson, A., Flood, B., Frölind, P.-O., Hellsten, H., Jonsson, T., Larsson, B., Stenström, G., and L.M.H. Ulander, Development and Operation of the FOA CARABAS HF/VHF-SAR System, Proc. 4th international workshop on Radar Polarimetry, Nantes, France, 13-17 July, pp. 214-228, 1998

[5] Miller, T., Potter, L., and J. McCorkle, RFI Suppression for Ultra Wideband Radar, IEEE Transactions on Aerospace and Electronic Systems, vol. 33, pp. 1142-1156, 1997

[6] Luo, X., Ulander, L.M.H., Askne, J., Smith, G., and P.-O. Frölind, RFI Suppression in Ultra-Wideband SAR Systems Using LMS Filters in Frequency Domain, Electronics Letters, vol. 37, pp. 241-243, 2001

[7] Ulander, L.M.H., Performance of Stepped-Frequency Waveform for Ultra-Wideband VHF SAR, Proc. EUSAR'98, Friedrichshafen, Germany, 25-27 May 1998, pp. 323-328, 1998

[8] Ulander, L.M.H., and P.-O. Frölind, Precision Processing of CARABAS HF/VHF-band SAR Data, Proc. IGARSS´99, Hamburg, Germany, 1999, 28 June - 2 July 1999, pp. 47-49, 1999

[9] Ulander, L.M.H., Hellsten, H., and G. Stenström, Synthetic-Aperture Radar Processing Using Fast Factorised Backprojection, Proc. EUSAR 2000, Munich, Germany, 23-25 May 2000, pp. 753-756, 2000

[10] Ulander, L.M.H., Frölind, P.-O., and T. Martin, Processing and Calibration of Ultra-Wideband SAR Data from CARABAS-II, Proc. CEOS SAR Workshop, Toulouse, France, 26-29 October 1999, ESA SP-450, pp. 273-278, 1999

[11] Ulander, L.M.H., Accuracy of Using Point Targets for SAR Calibration, IEEE Trans. Aerospace Electron Syst., Vol.27, No.1, pp.139-148, 1991

[12] Ulander, L.M.H., Radiometric Slope Correction of Synthetic-Aperture Radar Images, IEEE Trans. Geosci. Remote Sensing, Vol.34, No.5, pp. 1115-1122, 1996

[13] Ulander, L.M.H., and T. Le Toan, Bragg-Scattering Resonance in VHF-SAR Forestry Data, Proc. IGARSS´99, Hamburg, Germany, 28 June - 2 July 1999, pp. 1886-1888, 1999

[14] Ulander, L.M.H., Frölind, P.-O., Gustavsson, A., Hellsten, H., and B. Larsson, Detection of Concealed Ground Targets in CARABAS SAR Images Using Change Detection, Proc. Algorithms for Synthetic Aperture Radar Imagery, SPIE AeroSense Conference, Orlando, FL, 5-9 April 1999, SPIE vol. 3721, pp. 243-252, 1999

[15] Gustavsson, A., Ulander, L.M.H., Frölind, P.-O., Jonsson, T., Larsson, B., Stenström, G., Le Coz, D., Du Plessis, O., and P. Martineau, Radar Imaging of Forested Areas during the RAMCAR98 SAR Experiment, Proc. RADAR 99, Brest, France, 17-21 May 1999

[16] Gustavsson, A., Ulander, L.M.H., Frölind, P.-O., Jonsson, T., Larsson, B., Stenström, G., Le Coz, D., Du Plessis, O., and P. Martineau, The French-Swedish Multi-Frequency SAR Campaign RAMCAR98, Proc. IGARSS´99, Hamburg, Germany, 28 June - 2 July 1999, pp. 2599-2603, 1999

[17] Melon, P., Le Toan, T., Floury, N., Martinez, J.M., and L.M.H. Ulander, Analysis of VHF SAR Data over Pine Forest, Proc. IGARSS´99, Hamburg, Germany, 28 June - 2 July 1999, pp. 1655-1657, 1999

[18] Melon, P., Martinez, J.M., Le Toan, T., Ulander, L.M.H., and A. Beaudoin, On the Retrieving of Forest Stem Volume from VHF SAR Data: Observation and Modelling, submitted to IEEE Trans. Geosci. Remote Sensing

Appendix A. CARABAS image examples

The file name is annotated to the right of each image and from the used syntax the flight mission and imaging pass can be retrieved according to the description in Chapter 4. All of the 22 image examples found on pages 42-63 have been radiometrically calibrated and have the same color map.

CARABAS-II VHF SAR: RAMCAR Nezer

Radar illumination

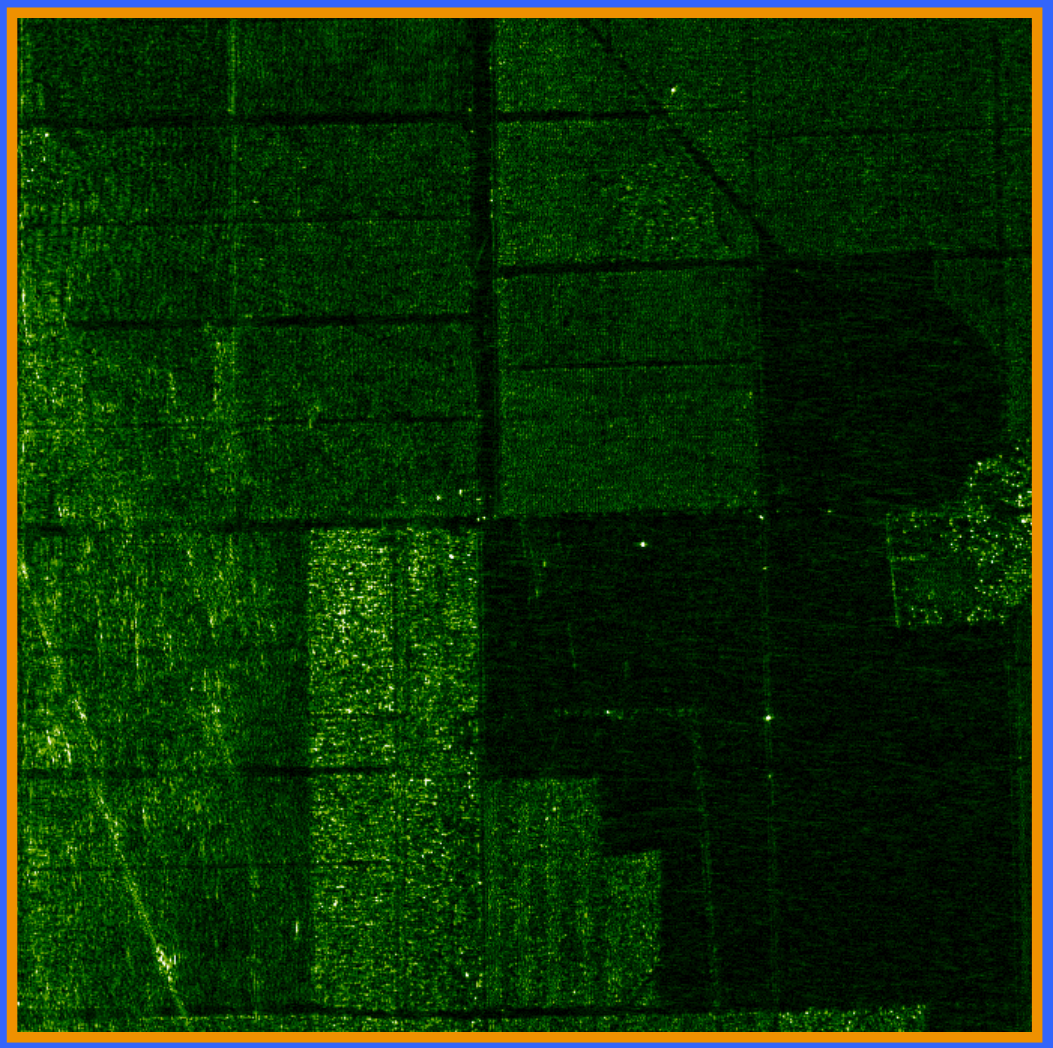

980512 1:1 Image fr98_1_1_15.Fac.RFcorr

Azimuth x Slant range
Size: 2048 x 2048 m^2
Resolution: 3 x 3 m^2
Band: 20-82 MHz
Incidence angle: 31º-56º

Figure A.1

FOI
SWEDISH DEFENCE RESEARCH AGENCY

FOI-R--0177--SE

CARABAS-II VHF SAR: RAMCAR Nezer

Radar illumination

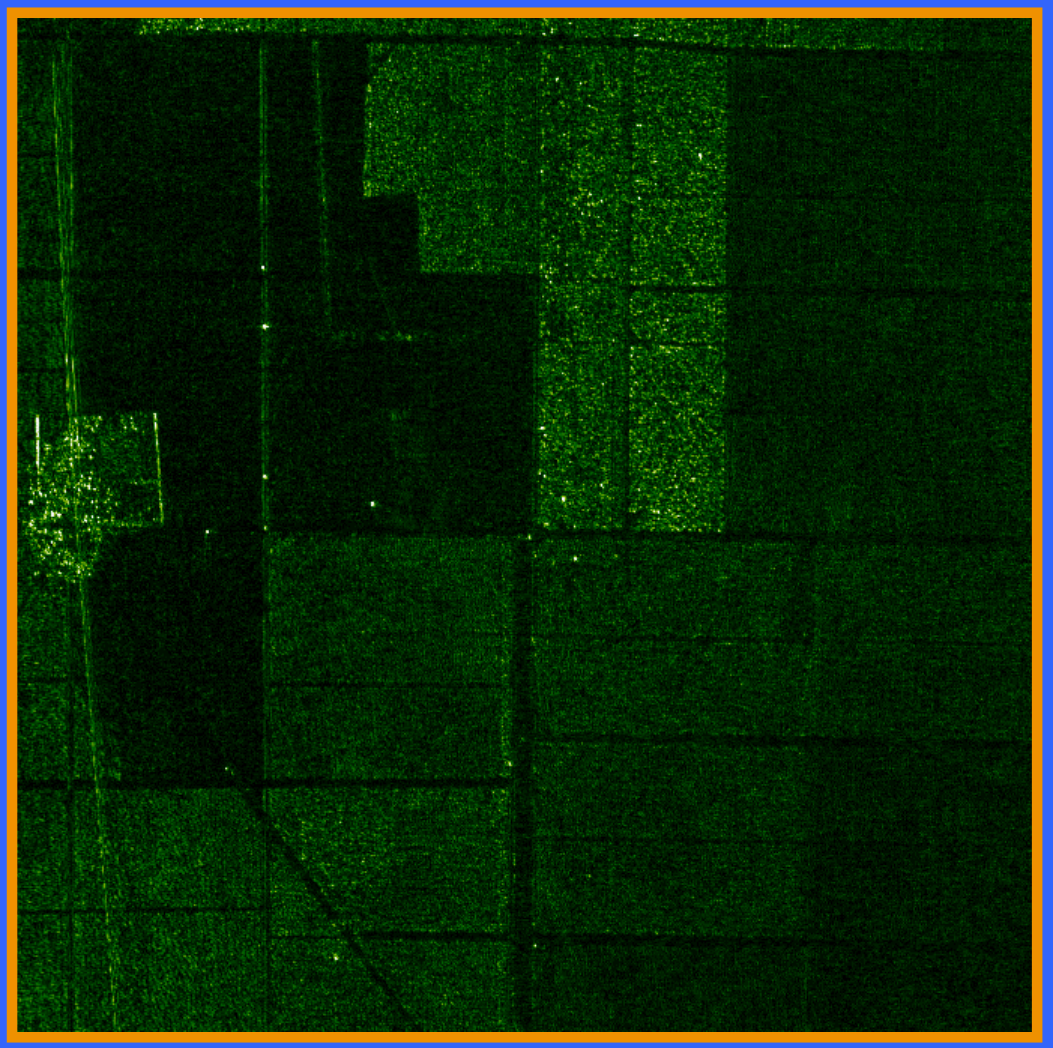

980512 1:2 Image fr98_1_2_11.Fac.RFcorr

Azimuth x Slant range
Size: 2048 x 2048 m^2
Resolution: 3 x 3 m^2
Band: 20-82 MHz
Incidence angle: 33º-57º

Figure A.2

FOI
SWEDISH DEFENCE RESEARCH AGENCY

FOI-R--0177--SE

CARABAS-II VHF SAR: RAMCAR Nezer

Radar illumination

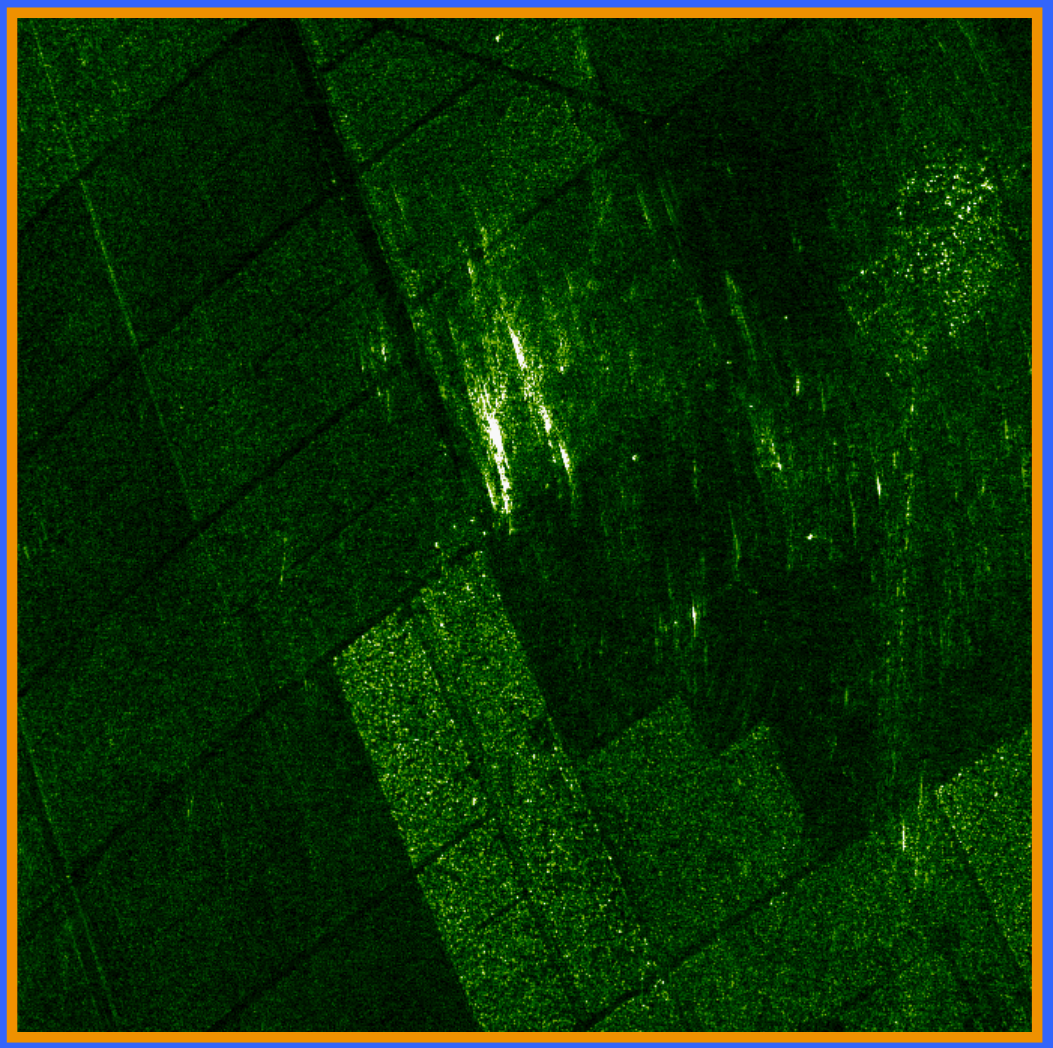

980512 1:3 Image fr98_1_3_5.Fac.RFcorr

Azimuth x Slant range
Size: 2048 x 2048 m^2
Resolution: 3 x 3 m^2
Band: 20-82 MHz
Incidence angle: 31º-57º

Figure A.3

FOI
SWEDISH DEFENCE RESEARCH AGENCY

FOI-R--0177--SE

CARABAS-II VHF SAR: RAMCAR Nezer

Radar illumination

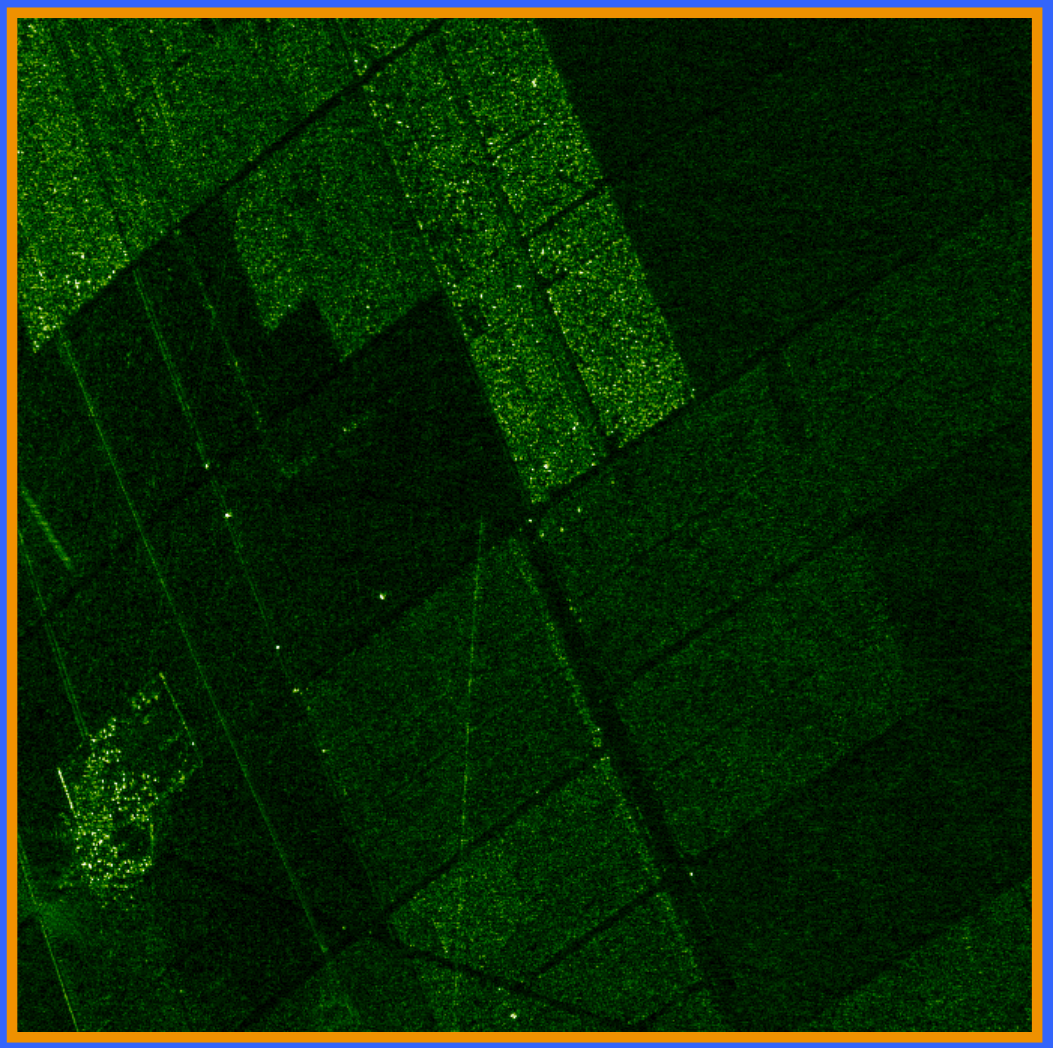

980512 1:4 Image fr98_1_4_5.Fac.RFcorr

Azimuth x Slant range
Size: 2048 x 2048 m^2
Resolution: 3 x 3 m^2
Band: 20-82 MHz
Incidence angle: 33º-57º

Figure A.4

FOI
SWEDISH DEFENCE RESEARCH AGENCY
FOI-R--0177--SE

CARABAS-II VHF SAR: RAMCAR Nezer

Radar illumination

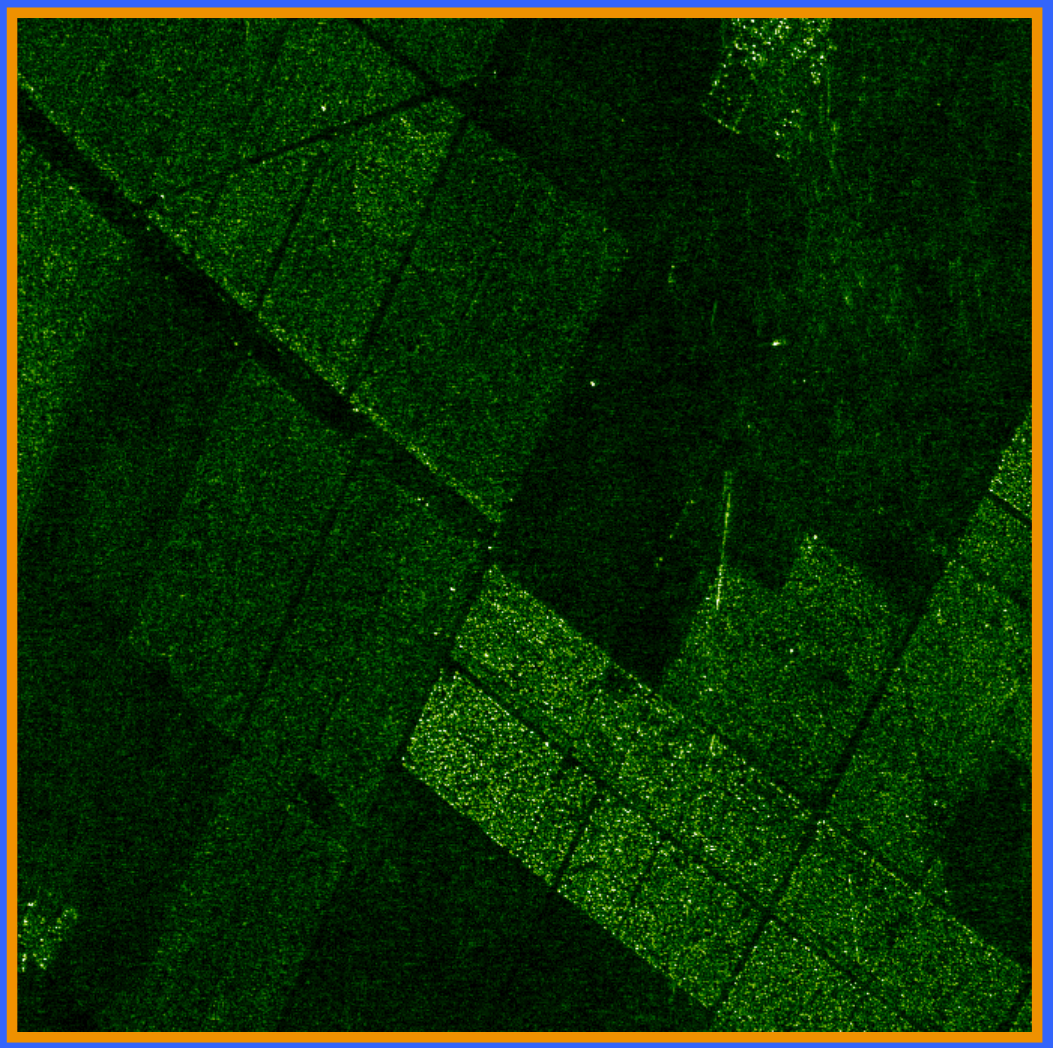

980512 1:5 Image fr98_1_5_3.Fac.RFcorr

Azimuth x Slant range
Size: 2048 x 2048 m^2
Resolution: 3 x 3 m^2
Band: 20-82 MHz
Incidence angle: 33º-57º

Figure A.5

FOI-R--0177--SE

FOI
SWEDISH DEFENCE RESEARCH AGENCY

CARABAS-II VHF SAR: RAMCAR Nezer

Radar illumination

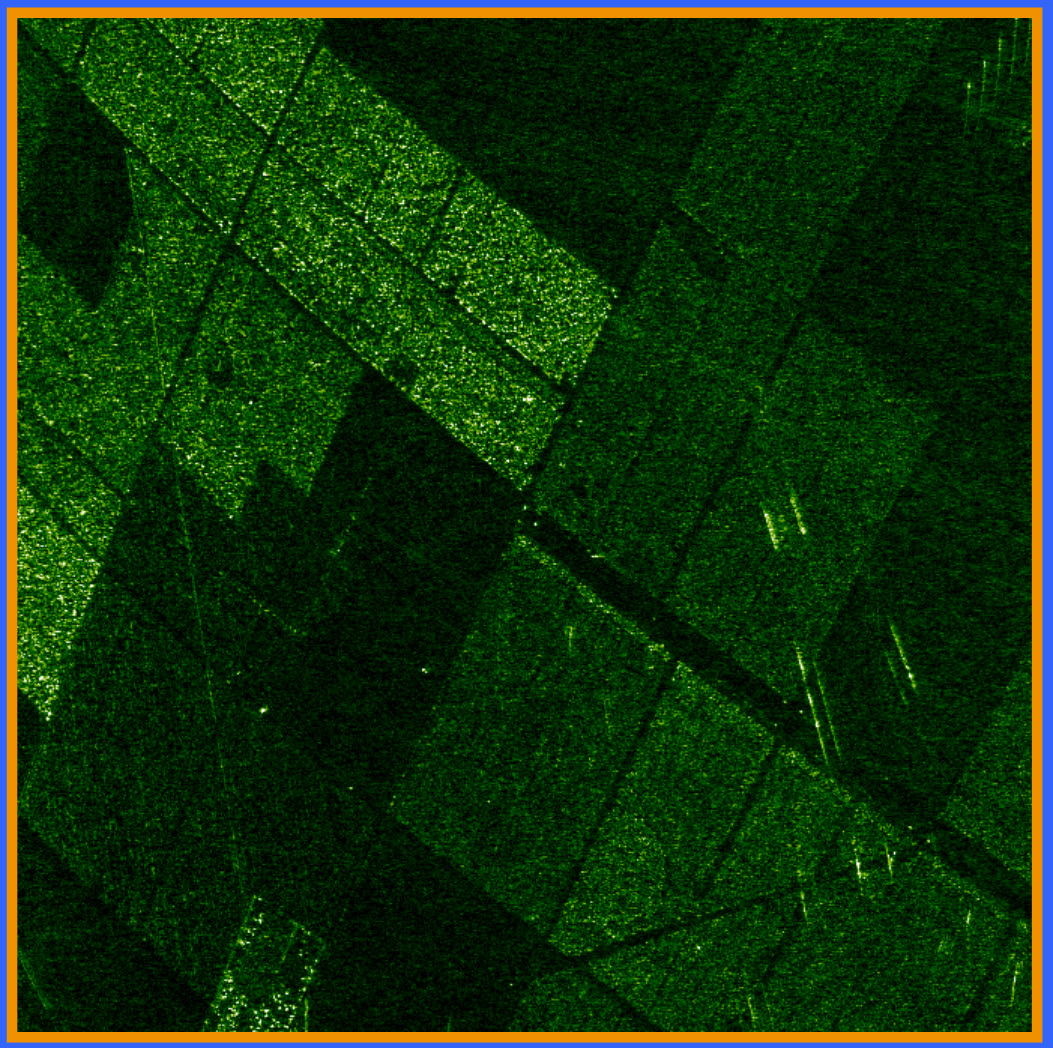

980512 1:6 Image fr98_1_6_2.Fac.RFcorr

Azimuth x Slant range
Size: 2048 x 2048 m^2
Resolution: 3 x 3 m^2
Band: 20-82 MHz
Incidence angle: 31º-57º

Figure A.6

FOI
SWEDISH DEFENCE RESEARCH AGENCY

FOI-R--0177--SE

CARABAS-II VHF SAR: RAMCAR Nezer

Radar illumination

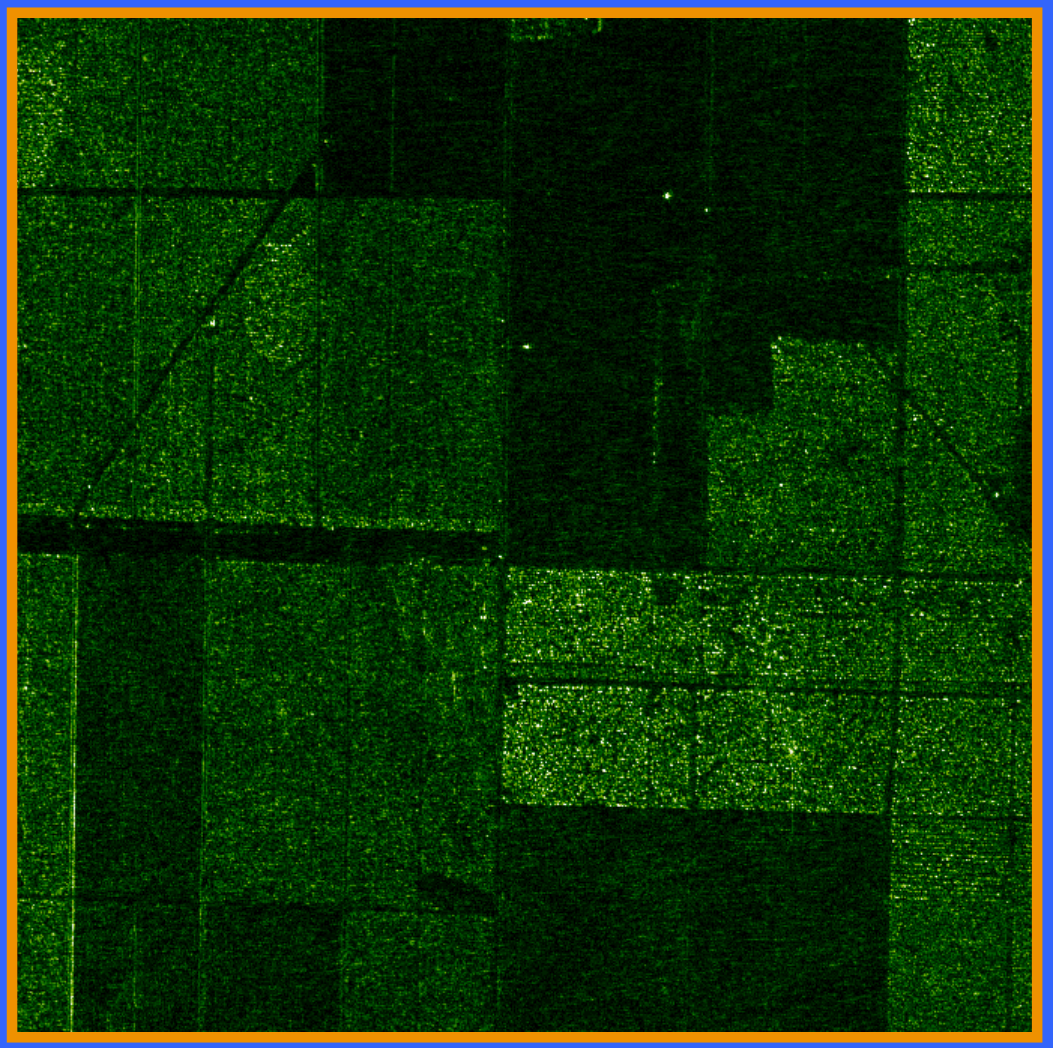

980512 1:7 Image fr98_1_7_8.Fac.RFcorr

Azimuth x Slant range
Size: 2048 x 2048 m^2
Resolution: 3 x 3 m^2
Band: 20-82 MHz
Incidence angle: 35º-58º

Figure A.7

FOI-R--0177--SE

FOI
SWEDISH DEFENCE RESEARCH AGENCY

CARABAS-II VHF SAR: RAMCAR Nezer

Radar illumination

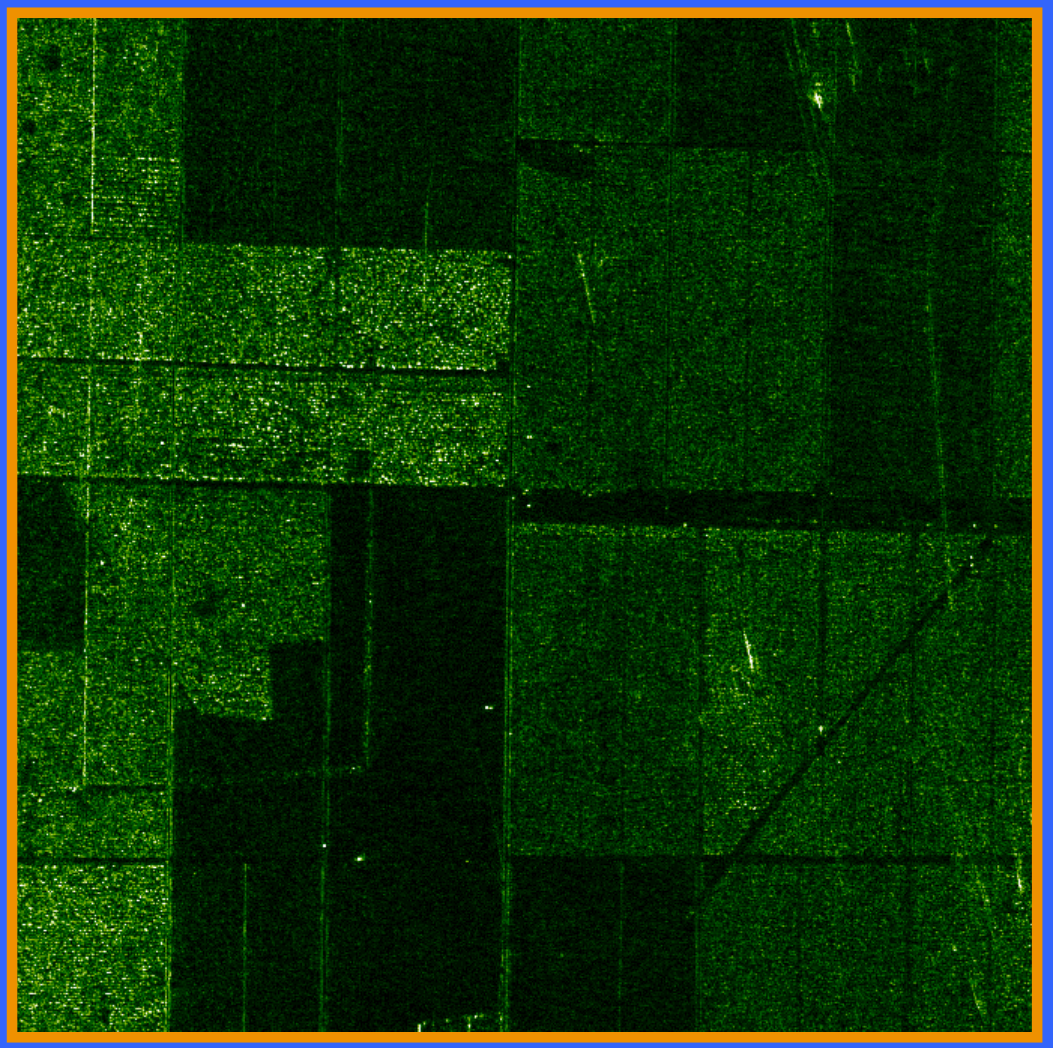

980512 1:8 Image fr98_1_8_6.Fac.RFcorr

Azimuth x Slant range
Size: 2048 x 2048 m^2
Resolution: 3 x 3 m^2
Band: 20-82 MHz
Incidence angle: 30º-56º

Figure A.8

FOI-R--0177--SE

FOI
SWEDISH DEFENCE RESEARCH AGENCY

CARABAS-II VHF SAR: RAMCAR Nezer

Radar illumination

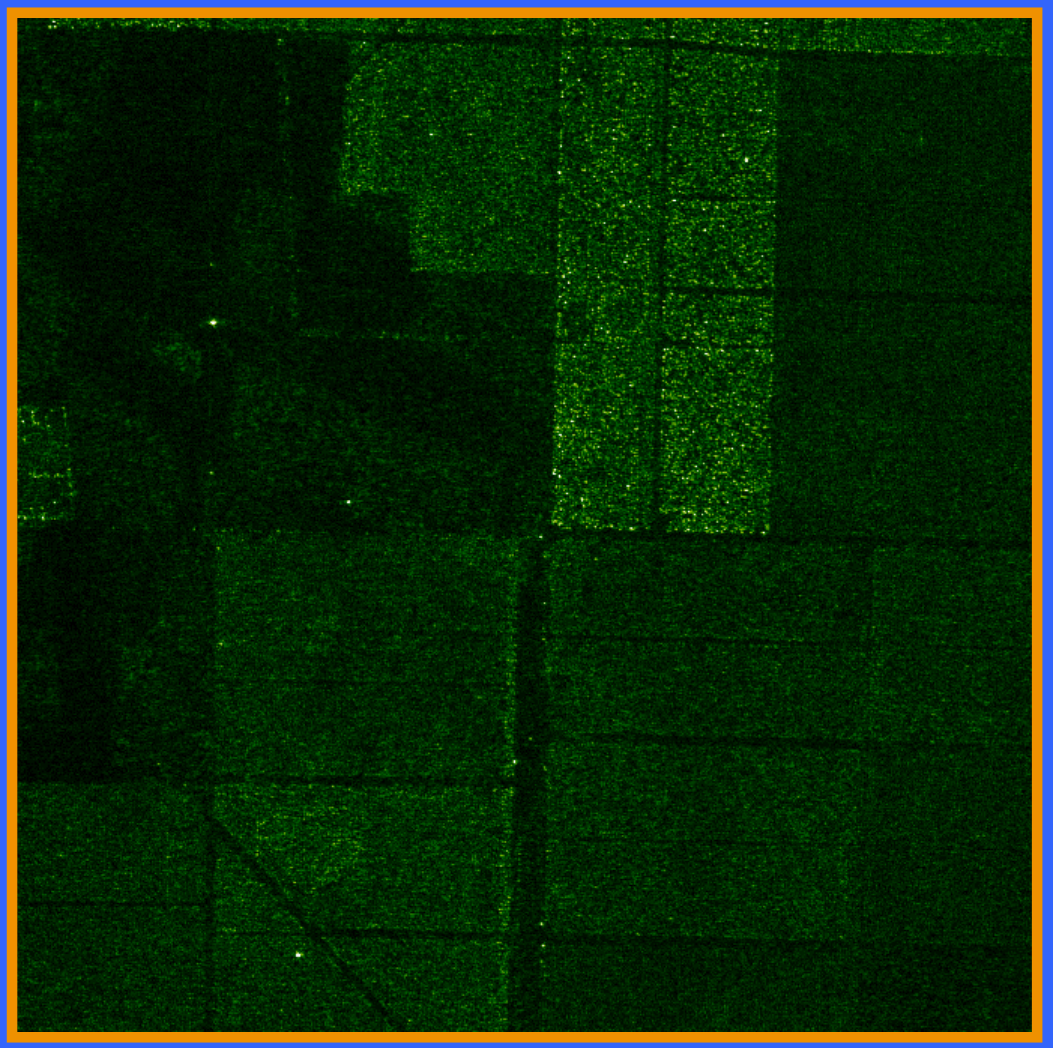

980512 1:9 Image fr98_1_9_12.Fac.RFcorr

Azimuth x Slant range
Size: 2048 x 2048 m^2
Resolution: 3 x 3 m^2
Band: 20-82 MHz
Incidence angle: 62º-69º

Figure A.9

FOI-R--0177--SE

FOI
SWEDISH DEFENCE RESEARCH AGENCY

CARABAS-II VHF SAR: RAMCAR Nezer

Radar illumination

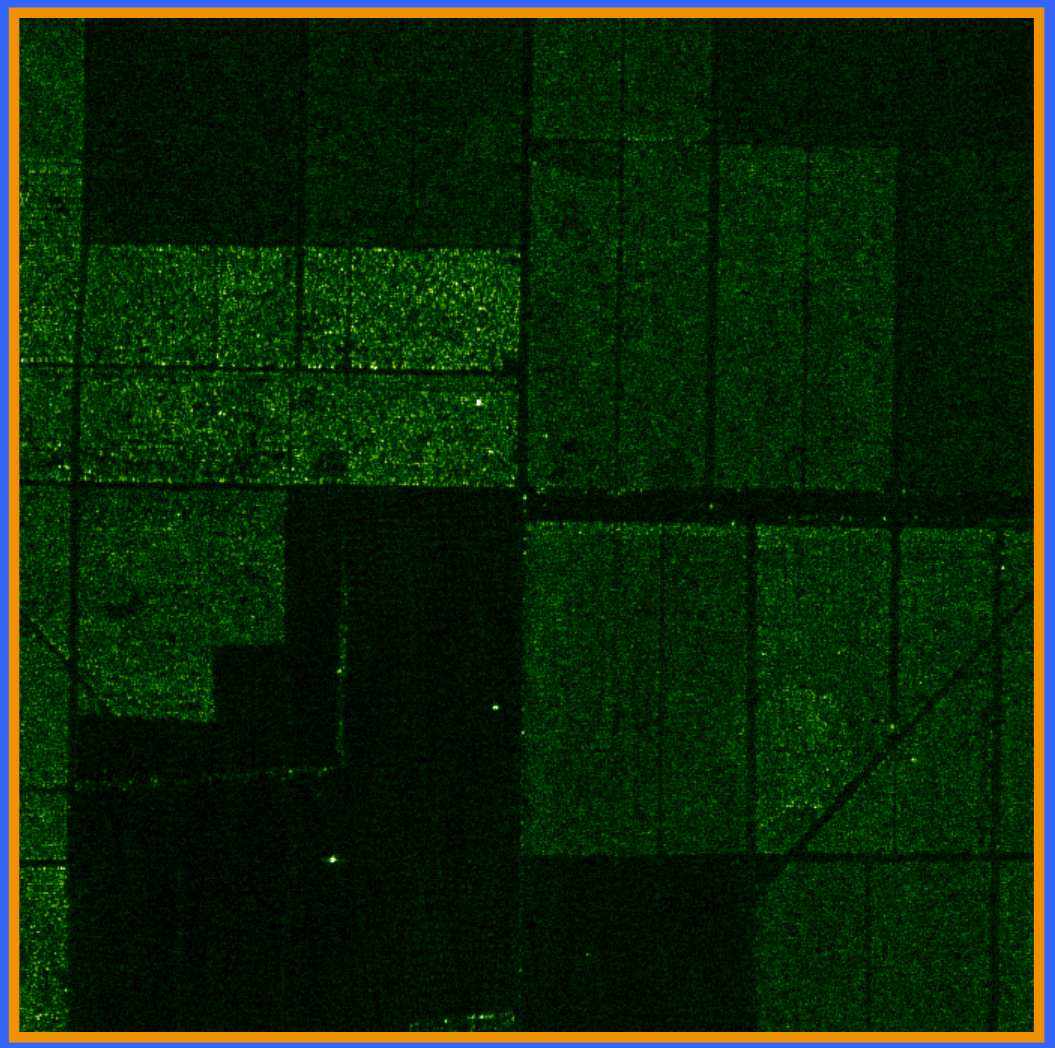

980512 1:10 Image fr98_1_10_3.Fac.RFcorr

Azimuth x Slant range
Size: 2048 x 2048 m^2
Resolution: 3 x 3 m^2
Band: 20-82 MHz
Incidence angle: 63º-69º

Figure A.10

FOI-R--0177--SE

FOI
SWEDISH DEFENCE RESEARCH AGENCY

CARABAS-II VHF SAR: RAMCAR Nezer

Radar illumination

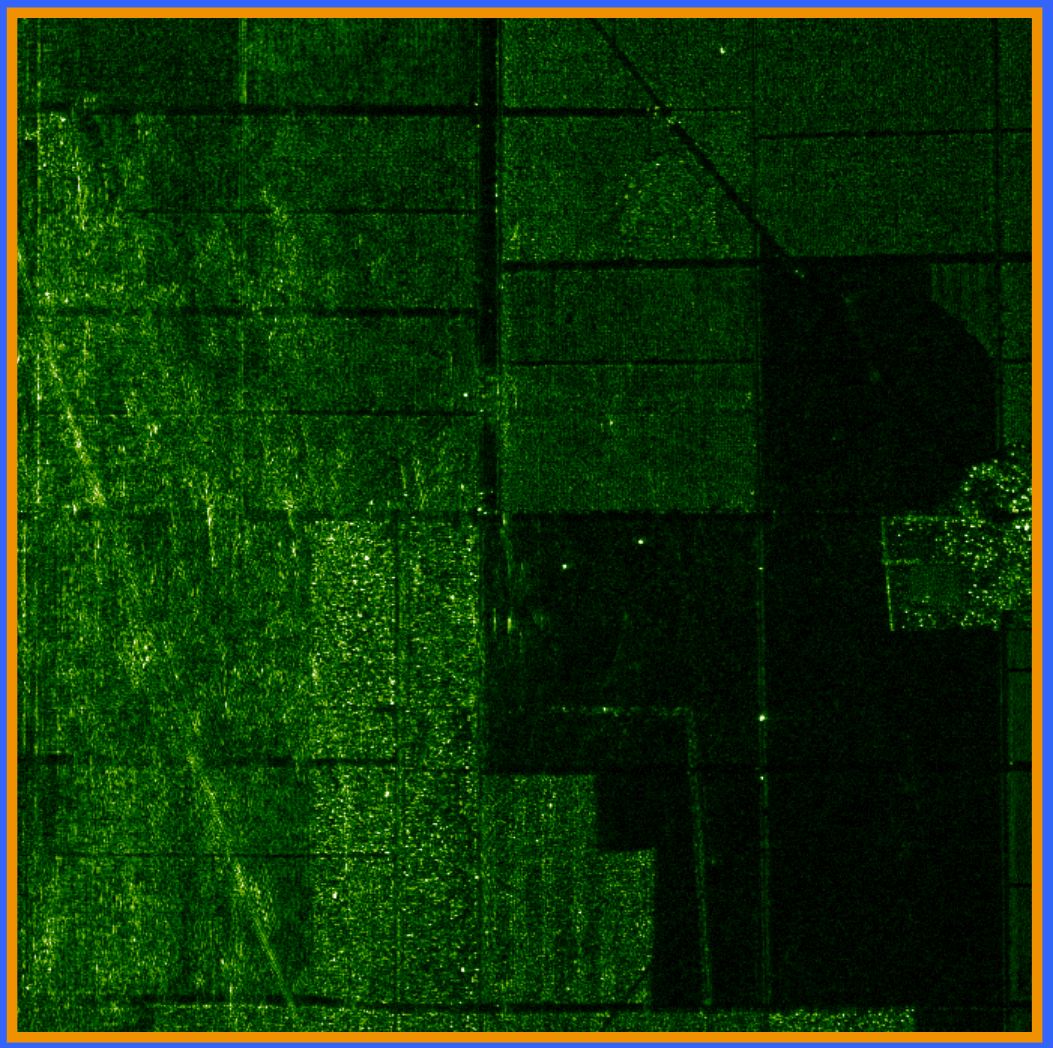

Azimuth x Slant range
Size: 2048 x 2048 m^2
Resolution: 3 x 3 m^2
Band: 20-82 MHz
Incidence angle: 28º-56º

Figure A.11

980514 2:1 Image fr98_2_1_18.a.Fbp.RFcorr

FOI-R--0177--SE

FOI
SWEDISH DEFENCE RESEARCH AGENCY

CARABAS-II VHF SAR: RAMCAR Nezer

Radar illumination

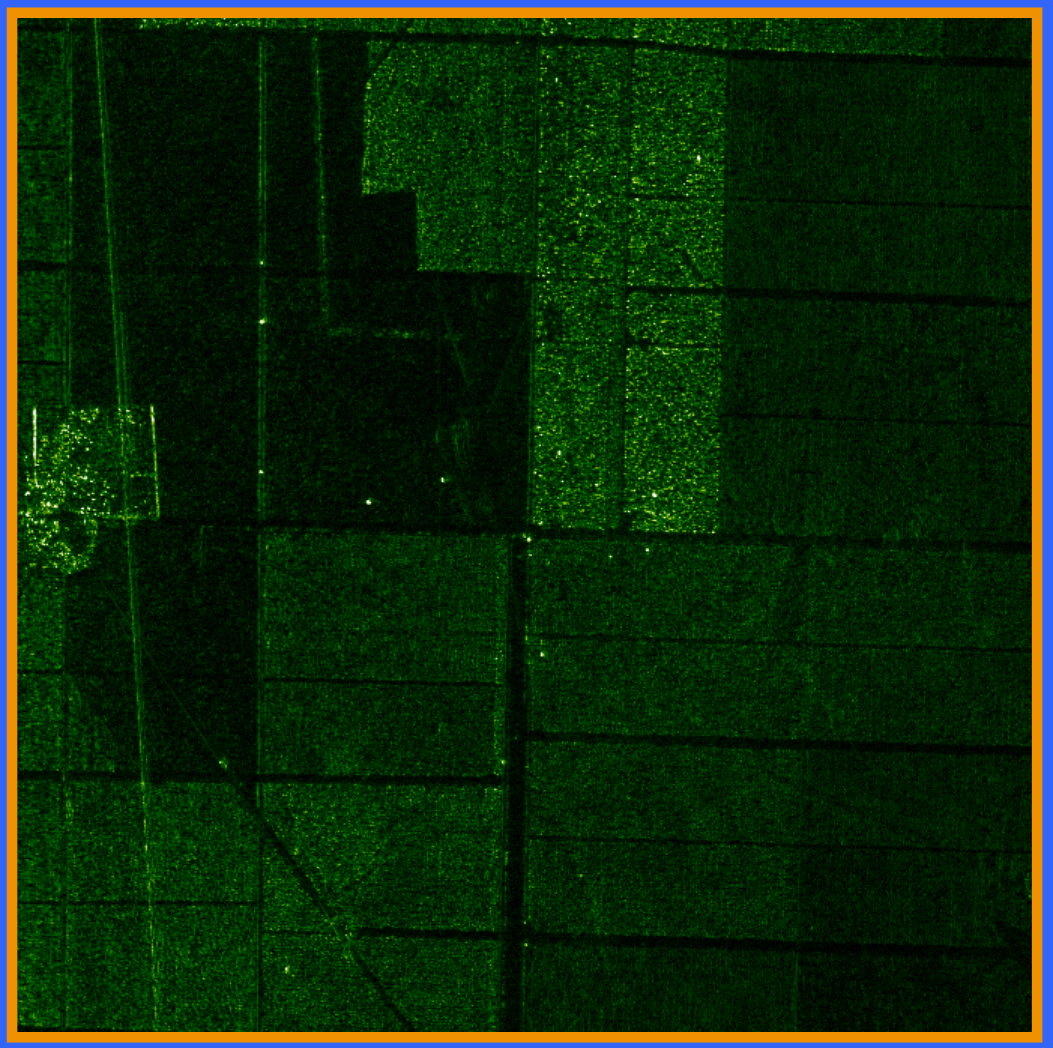

980514 2:2 Image fr98_2_2_9.a.Fbp.RFcorr

Azimuth x Slant range
Size: 2048 x 2048 m^2
Resolution: 3 x 3 m^2
Band: 20-82 MHz
Incidence angle: 33º-57º

Figure A.12

FOI-R--0177--SE

FOI
SWEDISH DEFENCE RESEARCH AGENCY

CARABAS-II VHF SAR: RAMCAR Nezer

Radar illumination

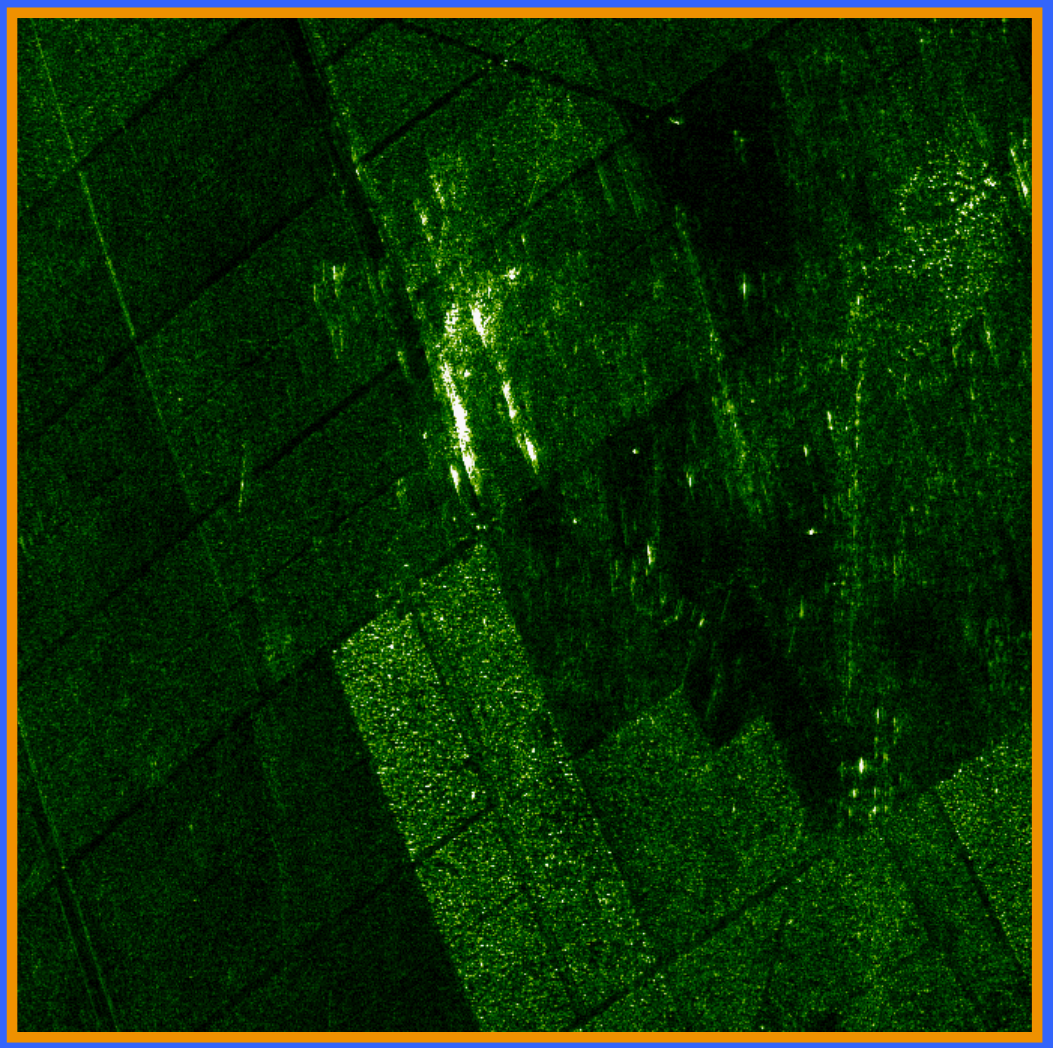

980514 2:3 Image fr98_2_3_6.a.Fbp.RFcorr

Azimuth x Slant range
Size: 2048 x 2048 m^2
Resolution: 3 x 3 m^2
Band: 20-82 MHz
Incidence angle: 32º-57º

Figure A.13

FOI-R--0177--SE

FOI
SWEDISH DEFENCE RESEARCH AGENCY

CARABAS-II VHF SAR: RAMCAR Nezer

Radar illumination

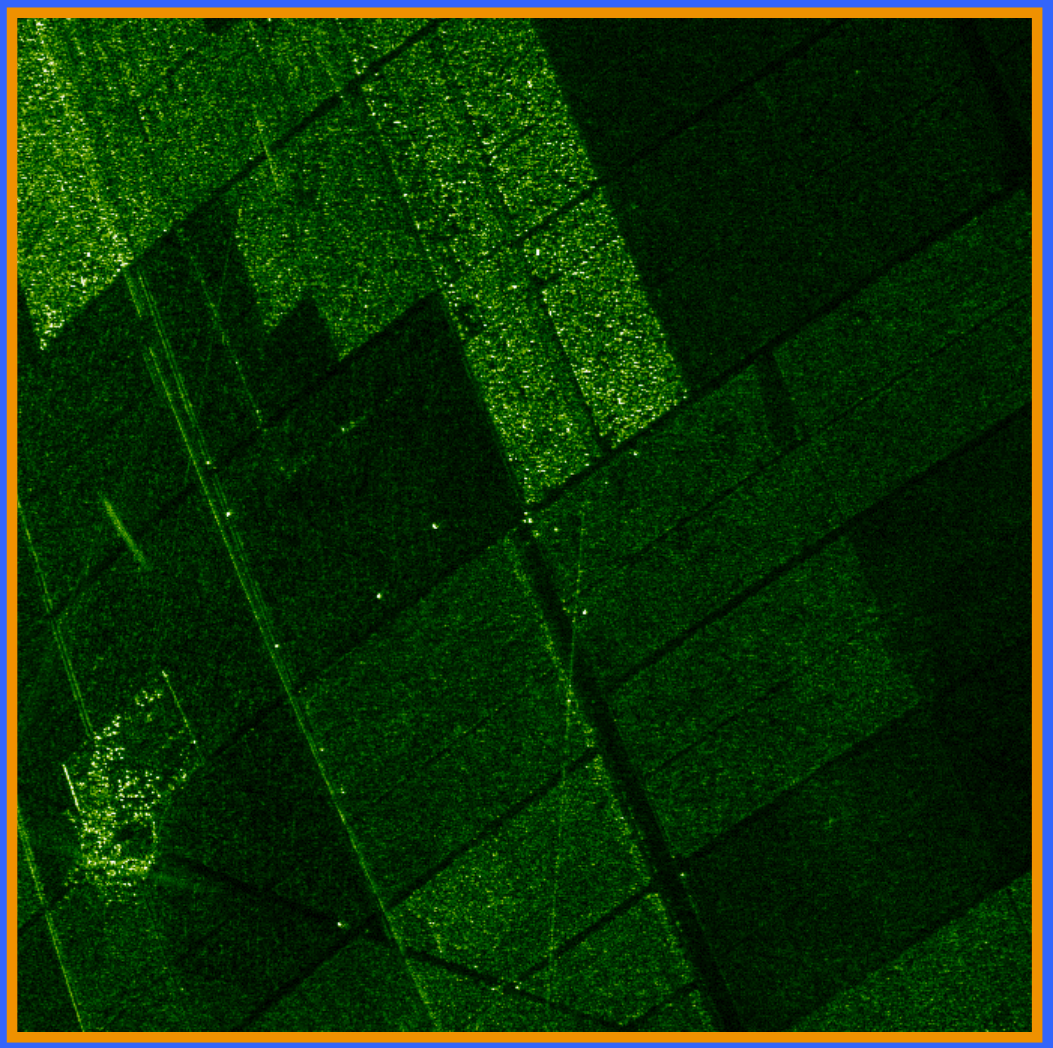

980514 2:4 Image fr98_2_4_6.a.Fbp.RFcorr

Azimuth x Slant range
Size: 2048 x 2048 m^2
Resolution: 3 x 3 m^2
Band: 20-82 MHz
Incidence angle: 31º-56º

Figure A.14

FOI-R--0177--SE

FOI
SWEDISH DEFENCE RESEARCH AGENCY

CARABAS-II VHF SAR: RAMCAR Nezer

Radar illumination

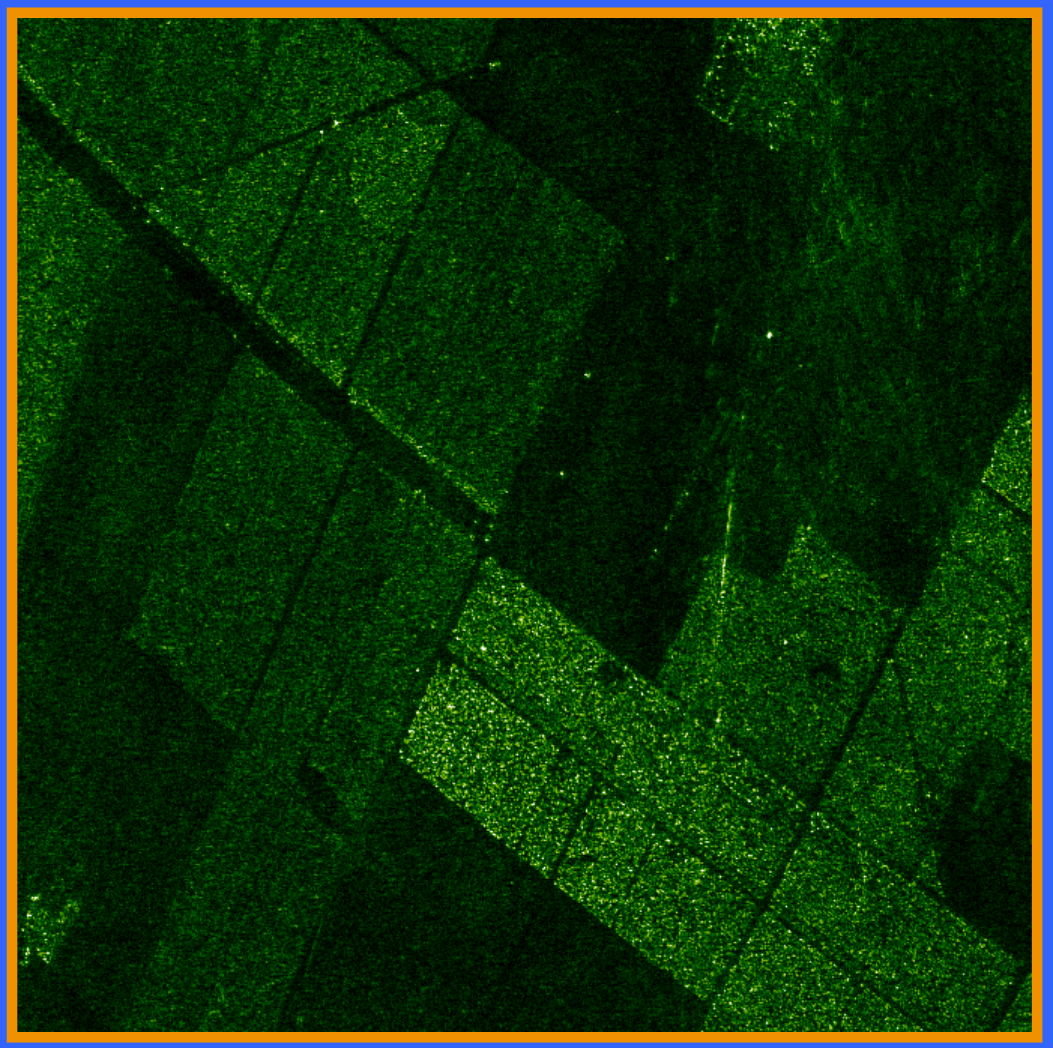

980514 2:5 Image fr98_2_5_6.a.Fbp.RFcorr

Azimuth x Slant range
Size: 2048 x 2048 m^2
Resolution: 3 x 3 m^2
Band: 20-82 MHz
Incidence angle: 31º-56º

Figure A.15

FOI
SWEDISH DEFENCE RESEARCH AGENCY

FOI-R--0177--SE

CARABAS-II VHF SAR: RAMCAR Nezer

Radar illumination

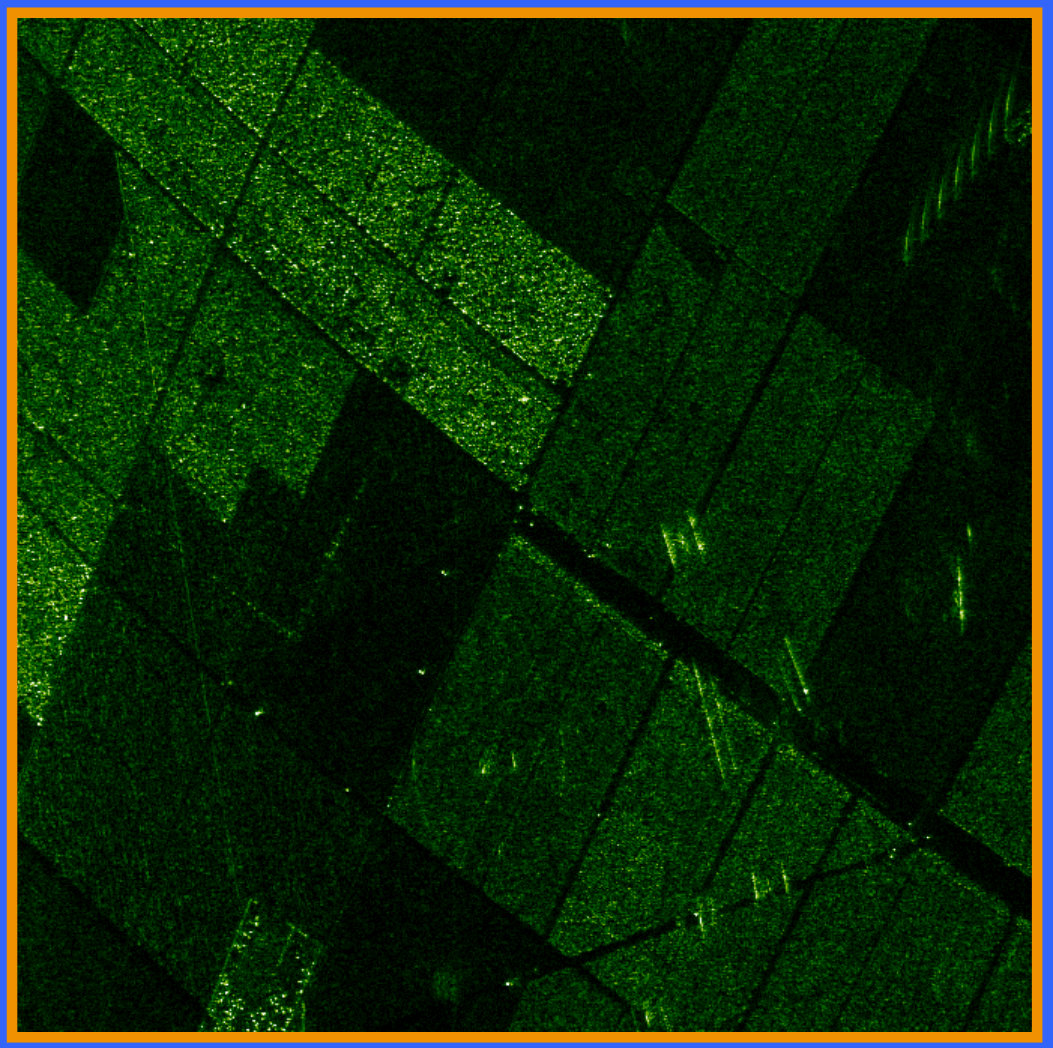

980514 2:6 Image fr98_2_6_5.a.Fbp.RFcorr

Azimuth x Slant range
Size: 2048 x 2048 m^2
Resolution: 3 x 3 m^2
Band: 20-82 MHz
Incidence angle: 32º-57º

Figure A.16

FOI
SWEDISH DEFENCE RESEARCH AGENCY

FOI-R--0177--SE

CARABAS-II VHF SAR: RAMCAR Nezer

Radar illumination

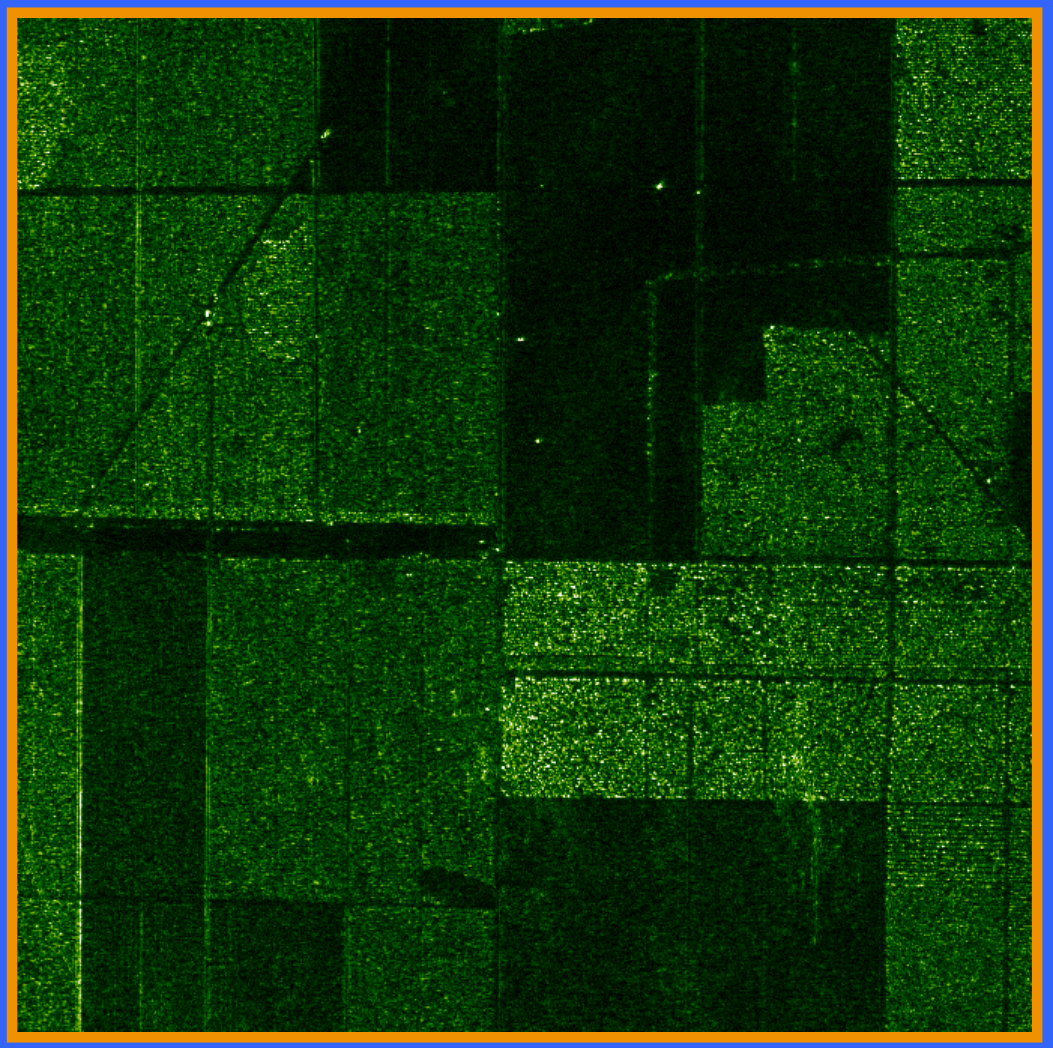

Azimuth x Slant range
Size: 2048 x 2048 m^2
Resolution: 3 x 3 m^2
Band: 20-82 MHz
Incidence angle: 34º-57º

Figure A.17

980514 2:7 Image fr98_2_7_6.a.Fbp.RFcorr

FOI-R--0177--SE

FOI
SWEDISH DEFENCE RESEARCH AGENCY

CARABAS-II VHF SAR: RAMCAR Nezer

Radar illumination

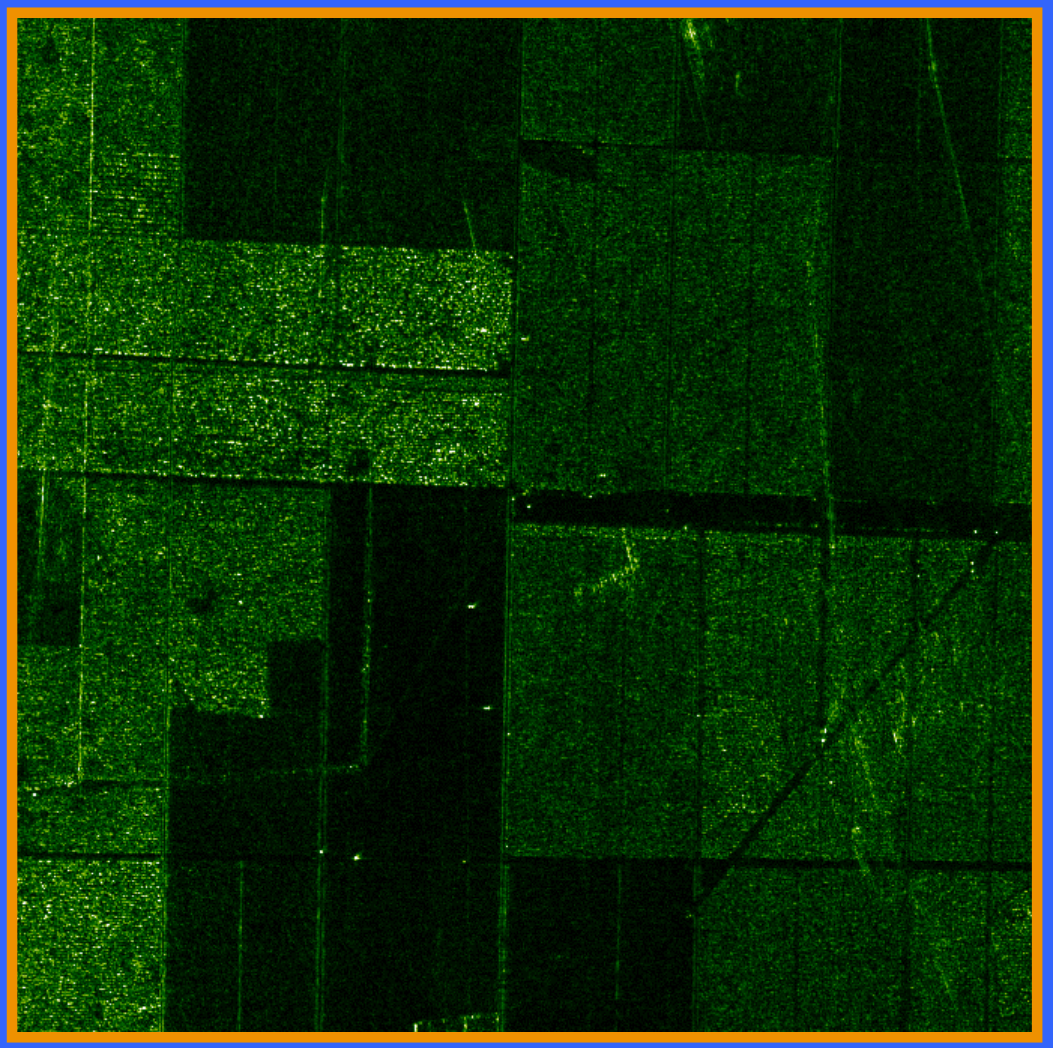

Azimuth x Slant range
Size: 2048 x 2048 m^2
Resolution: 3 x 3 m^2
Band: 20-82 MHz
Incidence angle: 31º-56º

Figure A.18

980514 2:8 Image fr98_2_8_7.a.Fbp.RFcorr

FOI-R--0177--SE

FOI
SWEDISH DEFENCE RESEARCH AGENCY

CARABAS-II VHF SAR: RAMCAR Causse Mende

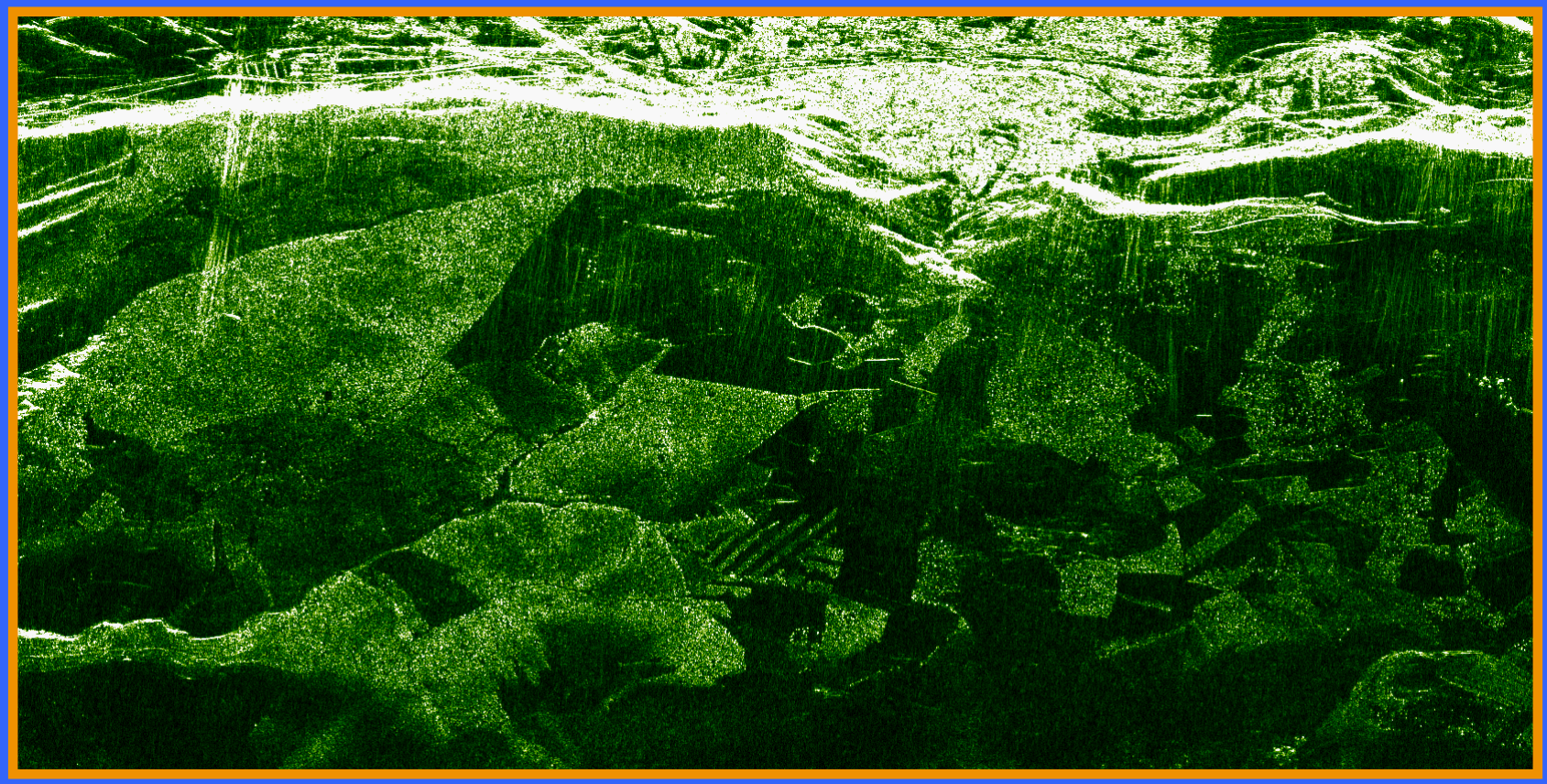

Azimuth x Slant range
Size: 5000 x 2500 m²
Resolution: 3 x 3 m²
Band: 20-82 MHz
Incidence angle: 32º-55º

Radar illumination

Figure A.19

FOI
SWEDISH DEFENCE RESEARCH AGENCY

980519 4:1 Image fr98_4_1_11.Fac.RFcorr

FOI-R--0177--SE

09

CARABAS-II VHF SAR: RAMCAR Causse Mende

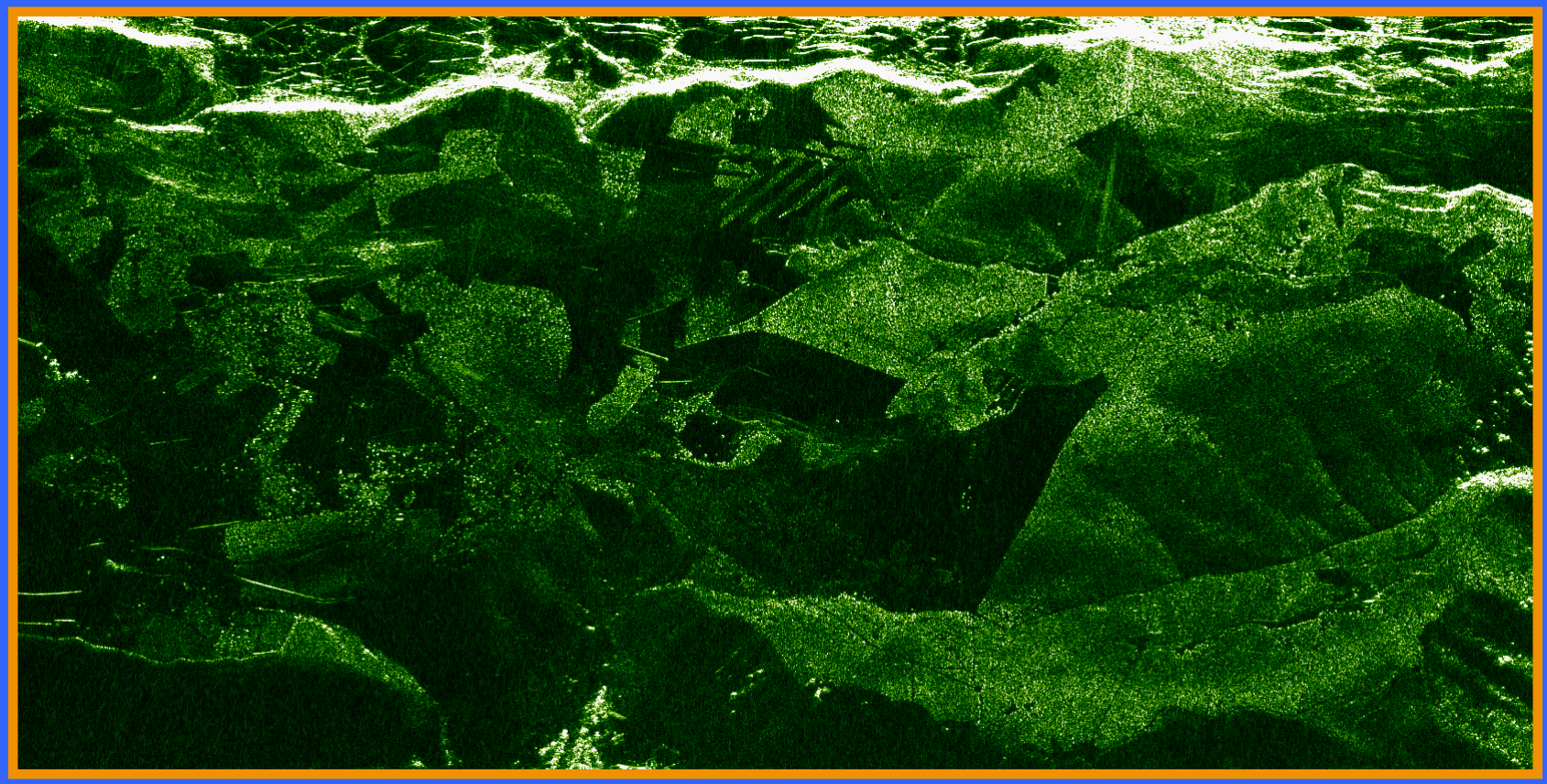

Azimuth x Slant range
Size: 5000 x 2500 m²
Resolution: 3 x 3 m²
Band: 20-82 MHz
Incidence angle: 36º-58º

Radar illumination

Figure A.20

FOI
SWEDISH DEFENCE RESEARCH AGENCY

980519 4:2 Image fr98_4_2_10.Fac.RFcorr

FOI-R--0177--SE

61

CARABAS-II VHF SAR: RAMCAR Causse Mende

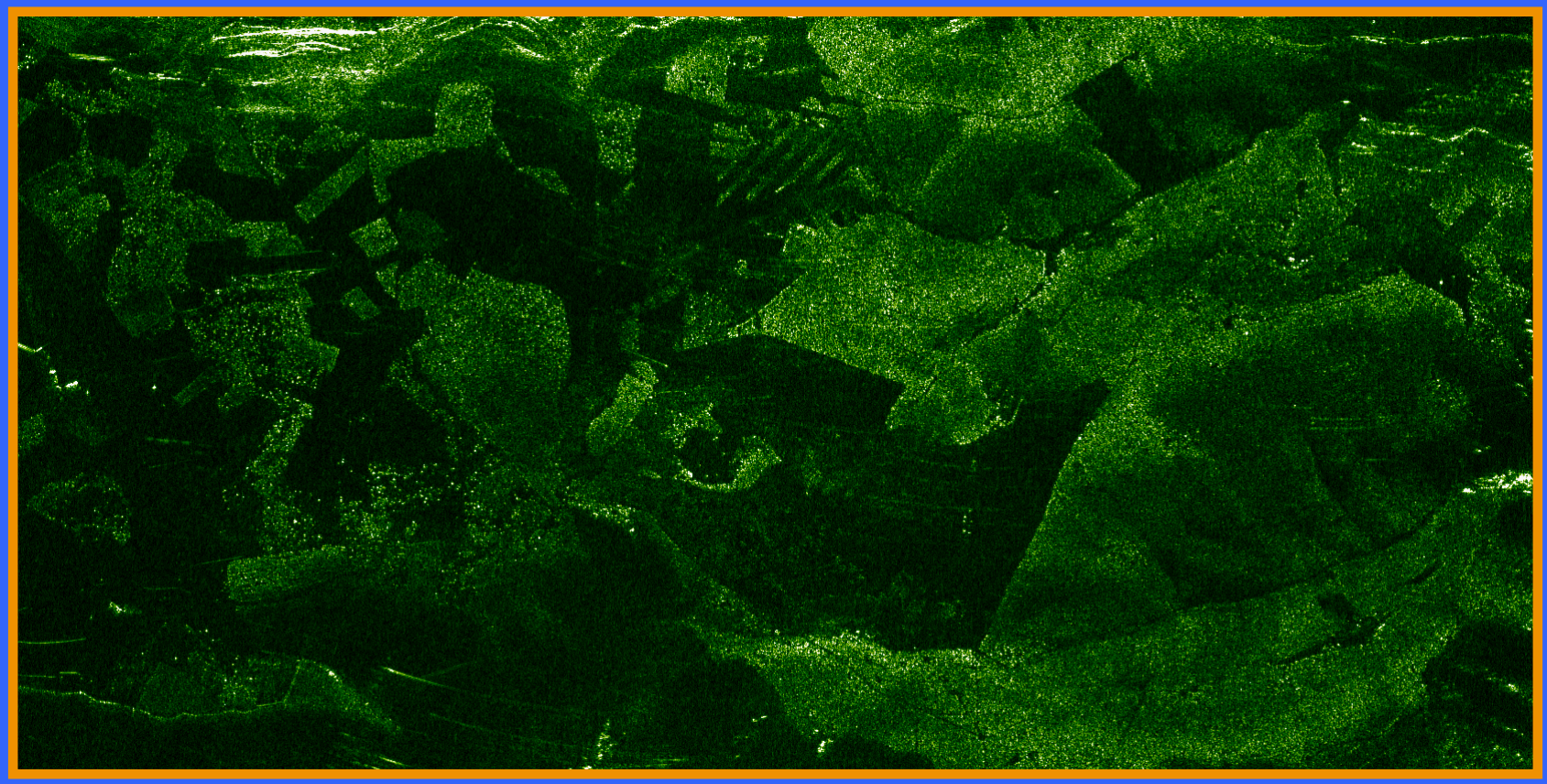

980519 4:5 Image fr98_4_5_12.Fac.RFcorr

Azimuth x Slant range
Size: 5000 x 2500 m²
Resolution: 3 x 3 m²
Band: 20-82 MHz
Incidence angle: 63º-69º

Radar illumination

Figure A.21

FOI
SWEDISH DEFENCE RESEARCH AGENCY

FOI-R--0177--SE

CARABAS-II VHF SAR: RAMCAR Causse Mende

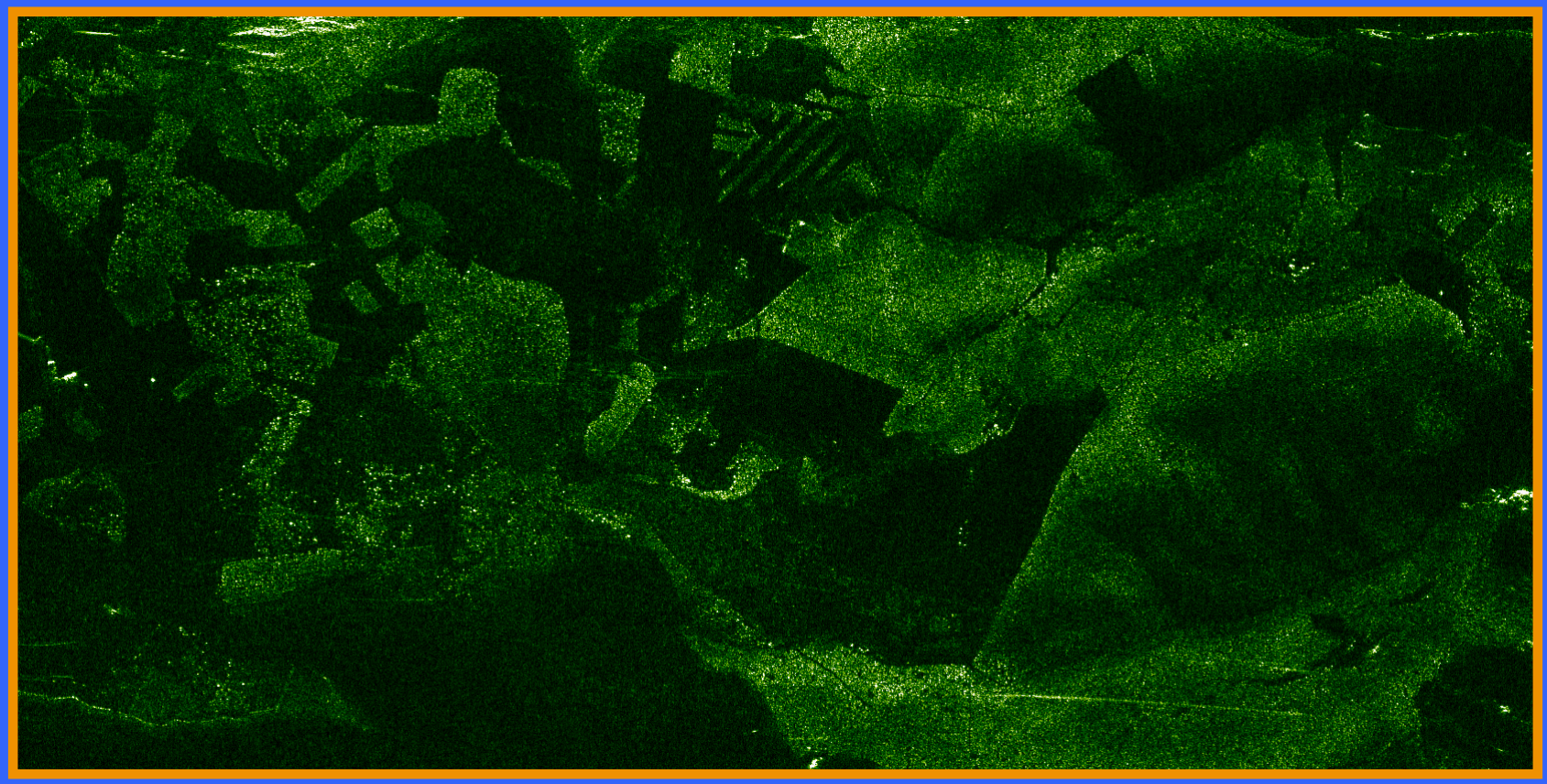

980519 4:7 Image fr98_4_7_5.Fac.RFcorr

Azimuth x Slant range
Size: 5000 x 2500 m²
Resolution: 3 x 3 m²
Band: 20-82 MHz
Incidence angle: 72º-75º

Radar illumination

Figure A.22

FOI
SWEDISH DEFENCE RESEARCH AGENCY

FOI-R--0177--SE